Wave Packet Dynamics In Parabolic Optical Lattice

A thesis submited in partial fulfillment of the requirement
for the degree of Master of Philosophy in Physics
Quaid-i-Azam University Islamabad.

Usman Ali

Department Of Physics
Quaid-i-Azam University
Islamabad, Pakistan
July, 2018.

Certificate

The undersigned hereby certify that they read and recommend to the Faculty of Graduate studies for the acceptance a thesis entitled ***"Wave Packet Dynamics In Parabolic Optical Lattice"*** by **Mr. Usman Ali** in partial fulfillment of the requirements for the degree of **Master of Philosophy**

Research Supervisor:

Prof. Dr. Farhan Saif
Department of Electronics
Quaid-I-Azam university
Islamabad Pakistan.

Submitted through:

Prof. Dr. Arif Mumtaz
Chairman
Department of Physics
Quaid-I-Azam university
Islamabad Pakistan.

Dedicated to my Parents.

Acknowledgements

All the praises to almighty ALLAH the most Merciful and Compassionate, the Sovereign power blessed me with knowledge; and able me to accomplish this work successfully and all respects for His Holy Prophet (PBUH).

I would like to express my sincere gratitude to my respectful supervisor Prof. Dr. Farhan Saif, for providing me an opportunity to work with him. I would especially like to thank him for continued guidance, support, motivation, patience and immense knowledge throughout the project. I have been extremely lucky to have a supervisor who cared so much about my work, and who responded to my questions and queries so promptly.

I would like to say especial thanks to Dr. Denys I. Bondar (Princeton University) and Dr. Joseph Pollard (University of Warwick) for their computational guidance. Both these persons helped me a lot in initial learning of *Python* programming language. Also I am thankful to all my group fellows, especially my research colleague Miss. Sara Medhat for their guidance in difficult times during whole session. I thank to all friends Ehsan Farooq, Javaid Hussain, Hamza Rehman, Mian Azeem and Abid Ali for novel discussions through out this session.

I feel strongly indebted to my parents, my family for their love, best wishes, encouragement and unconditional support without which I would have been unable to complete anything worth while.

I am grateful to Higher Education Commission, Government of Pakistan as well for the financial support through Indigenous Scholarship Scheme.

Abstract

A primer on the dynamics of ultracold atoms in parabolic optical lattices is presented. The general description of the system is not yet available. Although quasimomentum representation allows easy estimates of the eigenstates and energy spectrum, in the tight binding model. Exact behaviour of the eigenstates segregates the system evolution into two prominent dynamical modes, that are discerned as Bloch and Dipole oscillations.

The modes suffers, considerably, due to dephasing induced by unequal energy spacing of parabolic optical lattice. The corresponding atomic motions are heavily decohered, which resuscitates after certain periods due to periodic collapse and revival phenomenon.

It is also observed that the phenomenon of Landau-Zener tunnelling elicits over Bloch mode beyond single band approximation, which is of a particular character like never considered before. That is, the tunnelling fraction oscillates, instead to accelerate, and the wave packet dynamics interlace between Bloch and Dipole oscillations. The effects are explained from appropriate phase diagram for easy understandings.

Contents

List of Figures

List of Tables

Chapter 1

Introduction

Ultracold Physics is the most rapidly growing and versatile research area of physics, empirical side of which has leaped far beyond the conventional experiments of atomic, molecular and optical physics. The recent realization of ultracold molecules [Pérez-Ríos et al 2017] has opened new doors towards Biophysics and Quantum chemistry, with cold dipolar gases giving access to anisotropic interactions [Giannakeas et al 2013]. For the past couple of decades, manipulating ultracold atoms in optical lattices has been predominantly considered as the prime candidate for studying quantum many-body phenomena [Bloch et al 2008]. The use of Bose condensed atomic gases in this realm [Morsch and Oberthaler 2006] translate the complete matter wave picture of de Broglie on a hundred thousand times bigger screen. This also brings an excellent control of impurity free lattices which are totally artificial and fully customisable. Thus ultracold atoms is the leading quantum simulator [Gross 2017] from all the

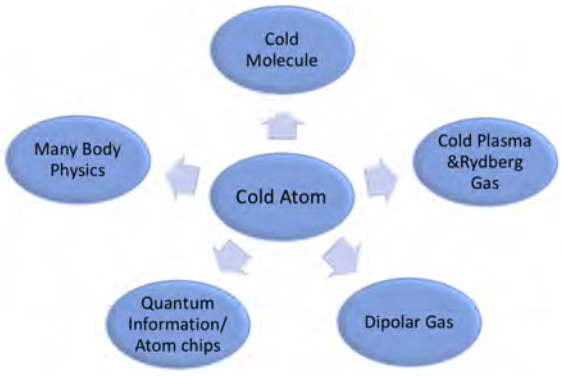

Trends in Ultracold Physics

present day technologies. Even the celebrated field of high energy physics can now be simulated at extremely low energies [Endres et al 2012] by lattice gauge theories in optical crystals [Goldman et al 2014; Zohar et al 2015]. Man's quest for practically observing fancy quantum world and making new devices with it [Gardiner and Zoller 2015] now seems possible on the grounds of ultracold physics, which has potential applications in the field of quantum control and quantum information [Jaksch 2007; Schneider 2012].

Like the famous saying, "Castles are not built in one day" all this had its genesis way back Galilean era, when Kepler surmised that comets experience a pressure from sun's radiations. In 1873 Maxwell derived analytical expressions of radiation pressure right after the Faraday's discovery of electromagnetic nature of light. First experimental evidence of mechanical action of light was on a metal foil by Lebedev [Lebedev 1901], repeated by Nichols [Nicholas and Hull 1903] who designed Nichols Radiometer for pressure measurements. Later on Lebedev [Lebedev 1910] extended his work by replacing metallic sheet with a diatomic molecule. Dirac and Kapitza [Kapitza and Dirac 1933] added more refinements to the field, by probing diffraction effects of electrons by stationary light waves.

The major outset came from a man who was not credited much for his providential work. Otto Frisch is the name we mainly know for the pioneering contributions to first atomic bomb. He was basically a nuclear physicist, who was first to detect fission by-products. But who knows that his experiment [Frisch 1933] for the measurement of atomic scattering from a resonant sodium light was inceptive to the field of atom optics. In this experiment recoil momentum gained while interatomic transitions causes the atoms to deflect. Interaction between light and atomic beams excites the atoms, also depositing some momentum component in addition. Since the spontaneous emission of photons is in arbitrary direction. Therefore, over each cycle net momentum conserves but atom experiences a force, known as spontaneous force or scattering force [Saif and Watanabe 2019]. This was the starting point, variants of which enabled trapping and cooling later on.

A super atomic state of matter at minimal temperatures was already been surmised by Bose and Einstein at that time. Although only deflection effects of atomic beams employing optical fields were made possible. The advent of laser in 1960 was a key technological advancement. In 1962 Askar'yan discerned another radiative force,

which was called the dipole force owing to the dipole moment induced by electric field. This force drives each atom towards regions of maximum or minimum intensity depending upon the phase between dipole moment and electric field. For a blue detuned incident field the direction of motion is towards intensity minima and opposite for red detuning. The physical phenomenon underneath is similar to atom field coupling explained by Jaynes and Cummings [Jaynes and Cummings 1963]. This laid the foundation of first atom trapping proposal by Letokhov [Letokhov 1968].

Art Ashkin [Ashkin 1970] utilized both these forces to trap small particles with a pair of counter propagating laser beams. This was a key turning point, which initiated a plethora of novel experiments for atom manipulation. The groups of Hansch [Hänsch 1975] and Wineland [Wineland 1975] segreggately proposed laser cooling schemes, where Hansch's work was purely concerned with cooling neutral atoms and Wineland's was more related to cooling and trapping of ions. Right from the beginning magnetic trapping was also running parallel, which were then employed for further confinement [Migdall et al 1985] and the trap so formed was named magneto optical trap (MOT) [Raab et al 1987]. Manipulating atoms now seemed easier and the problem of μK temperature limit was solved by almighty, when noble laureate William Philips noticed the discrepancy between measured and theoretically predicted temperature values [Gould et al 1987]. The atomic ensemble was found to be cold below the Doppler cooling limit. It was sisyphus cooling, already theorized [Dalibard and Cohen-Tannoudji 1985] with the physical significance of gradual energy loss while moving against potential hills. Westbrook [Westbrook et al 1990] reported first localization of atoms and hence optical lattices were realized.

Optical lattice paved the way towards fifth state of matter and soon after the implementation of evaporative cooling came the most fascinating experimental breakthrough of past vicennial. It was Bose-Einstein condensate [Anderson et al 1995; Bradley et al 1995; Davis and Blakie 2006] of interacting ultracold atoms in optical lattice, which is treated as super atom using appropriate particle statistics. Most of the celebrated phenomena of solid state electronic systems can now be simulated using ultracold atoms with precise control. The level of interest in the field gained momentum when it was observed that inter-atomic interaction can be tuned through magnetic [Courteille et al 2001; Inouye et al 1998] or optical [Theis et al 2004] Feshbach resonances [Chin et al 2010]. Interacting bosons and non-interacting fermions

of ultacold atoms can now coexist [Lewenstein et al 2004]. The ability to change the dimensionality of optical lattices, specially to generate periodic potentials, triggered the investigation of fancy quantum effects ascribed to coherent matter waves [Greiner et al 2002a; Saif 2005b]. It also enabled observation of celebrated solid state phenomena like band structure [Greiner et al 2001], Anderson localization [Roati et al 2008], Josephson junction [Gati 2007], quantum Hall effect [Palmer et al 2008], Bose-glass phase [Habibian et al 2013], superfluid to Mott-insulator transitions [Dubius 2009; Greiner et al 2002b], and more importantly the Bloch oscillations [Kolovsky and Korsch 2004]. Bloch oscillations and certain other effects in this domain has already contributed to high-precision determination of physical constants [Battesti et al 2004; Ramos et al 2017; Sacchetti 2017] with atomic clocks [Bloom et al 2014] providing stable and accurate time measurements.

In the present dissertation we focus on the elementary system of a 1D optical lattice in the presence of an external parabolic trap. The simplest experimental realization of 1D periodic potentials [Bloch 2005; Ott et al 2004a] requires additional atomic confinement, which reduces the dimensionality of 2D optical lattices to a quasi-1D optical lattice. The confining trap may be optical or magnetic and is similar to the dipole trap previously used for cooling and trapping [Lee et al 1996]. Thus the problem is instinctive and resembles to the quantum particle defined on a periodic lattice, superimposed by parabolic trapping potential, first thematisized by Mattis [Mattis 1986] for electronic motion in semiconductor superlattices. The parabolic potential is essential to confine the atoms, which constrains the atomic motion to a finite region of space and the lattice so formed is called parabolic optical lattice [Yamakoshi and Watanabe 2015]. The dynamics are totally non-intuitive with the combined potential substantially modifying the atomic motion, compared to systems where only one potential from the two exists, as shown theoretically [Hooley and Quintanilla 2004; Longhi 2007] and experimentally [Fertig et al 2005; Ott et al 2004b].

Coherent matter wave packets can easily be generated as well as manipulated in such potentials. The recent experiment done in Aarhus [Pedersen et al 2013] reports high fidelity production of wave packets of Bose condensed rubidium, which can be transferred to higher bands by lattice amplitude modulation [Medhat et al 2019; Yamakoshi et al 2018]. In our theoretical analysis we have considered such localized Bosonic wave packets, triggered by certain displacement of the trap origin. Single

particle problem has already been solved making use of special Mathieu functions [Rey et al 2005]. In contrast to previous studies, we employed accurate numerical and analytical techniques to determine exact energy spectrum and eigenstates of the system. Different regimes of energies and eigenstates are marked, which play crucial role in assigning wave packet dynamics.

Parabolic optical lattices have been eagerly studied owing to the localization of higher lying eigenstates away from the center of harmonic potential. Such localized eigenstates provide an ideal platform for precise quantum registers [Viverit et al 2004]. Localization of wave packet is also essential for observing celebrated quantum phenomenon of Bloch oscillations, whichever originate in a periodic potential under the influence of an external force [Bouchard and Luban 1995; Kolovsky and Korsch 2004]. Having understood the effect of dipole force arising from the optical or magnetic traps, it is quite instinctive that the presence of harmonic trap with quadratic forcing should modify Bloch oscillations [Geiger et al 2018]. Parabolic lattices satisfy both the preconditions. Hence Bloch dynamics are explored for the non-interacting ultracold Bosons.

Experimental advancements bring about the existence of truly 1D optical lattices making use of six counter propagating lasers, also known as modulated optical tubes. Such 1D arrays have their own interest as they enable investigation of Dipole oscillations of ultracold atoms. The difference between dipolar dynamics in truly and quasi-1D optical lattice has been revealed experimentally [Cataliotti et al 2003; Fertig et al 2005]. The secondary aim of present work is to analyse these effects.

Robust numerical methods have been used for the simulations of wave packet propagation. The numerical results go hand in hand with the theoretical predictions, meanwhile highlighting some notable dynamical features, never considered before in the course of parabolic optical lattices. That is, the wave packet undergoes fractional loss of probability amplitude to higher bands, ascribed to Landau-Zener tunnelling [Tayebirad et al 2010]. The tunnelling observed here produces oscillations instead of acceleration and the overall dynamics results in the interplay between Bloch and Dipole oscillations.

In short, parabolic optical lattice is the core of rich dynamical phenomena which are experimentally verified and workable in plentiful applications.

The work is organised as follows:

Chapter 2 mainly introduces the fundamental physics and basic understanding of cold Bosonic atoms in optical lattices. The primary aspects of trapping and manipulation of ultracold atoms in artificially engineered periodic crystals are presented, briefly discussing the role of additional parabolic potential.

Chapter 3 develops a firm understanding of Bloch oscillations in the single band approximation, considering the linear system. The phenomenon extends to quadratic forcing where we encounter Dipole oscillations in addition. Mean atomic observables are calculated using Heisenberg picture, which aids in developing simplified interpretation of system dynamics.

Chapter 4 primarily relates with tight binding description of single particle problem. Single-particle properties are practically attained for certain cold atomic gases by adjusting the inter-atomic s-wave scattering length to zero, utilizing Feshbach resonances. Single particle energy spectrum acts as a base line for further studies, by which borders of the system's dynamics are identified. This knowledge defines the basis to study the effect of system parameters on the general dynamics.

Chapter 5 covers the overall dynamics beyond all approximations. Wave packet propagation accentuate the emergence of Landau-Zener tunnelling on top of Bloch oscillations. The phenomenon is explained on the basis of band structure involved. The tunnelling observed here is completely different from previously observed effects. This is an important outcome of our studies.

Results are summarized and concluded in **Chapter 6**, making use of appropriate phase diagram.

Chapter 2

Parabolic Optical Lattice

The basic unifying element of ultracold physics is the optical lattice. The interference carpet of standing wave laser field generates "potential landscape", in which trapped entities move, posited by Letokhov [Letokhov and Minogin 1977]. Particularly for sufficiently coold atoms, the associated matter wave frequency commensurate with optical laser frequencies. Thus, even the atomic motion in optical crystals is within the realm of quantum physics. Right from the beginning a parabolic dipole trap is playing an imperitive role in most of the trapping experiments. The parabolic confining potential is also utilized over optical lattice while loading and transference processes of trapped entities. This significantly revamps the overall potential profile giving rise to finite parabolic lattice geometries, that are introduced in this chapter. Before moving to the context of the central physical aspects of this chapter, we shortly discuss optical lattice with various one-dimensional assemblies.

2.1 Optical Lattice

The stationary wave providing potential platform for atomic motion can be produced either by shining counter propagating lasers of same amplitude or by retro-reflection of a single laser beam. We considered the former with a pair of circularly polarized laser beams counter-shined from opposite directions, as shown in Fig. 2.1. Taking the unit vectors in three-dimensional cartesian coordinates, represented by $\{e_1, e_2, e_3\}$, we write the spatial profiles of both traveling waves as $\mathbf{E_1} \propto e^{ik_L x}[\cos(\varphi)\hat{e_3} + \sin(\varphi)\hat{e_2}]$ and $\mathbf{E_2} \propto e^{-ik_L x}[\cos(\varphi)\hat{e_3} - \sin(\varphi)\hat{e_2}]$, respectively. The net electric field in traveling

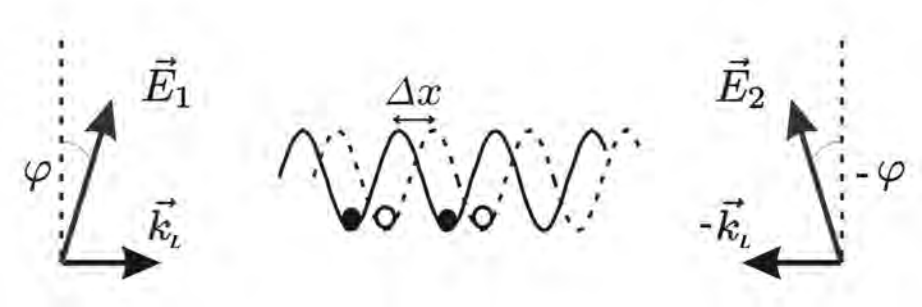

Figure 2.1: A schematic illustration of Laser configuration in generating mutable optical potentials [Jaksch and Zoller 2004]. Couple of standing waves generated by a pair of counter-shined laser beams are shown at a polarization angle of 2φ. Both potential landscapes are displaced at $\Delta x = 2\varphi/k_L$, which is tunable to generate different potential forms.

wave approximation is given by $\mathbf{E_1} - \mathbf{E_2} \propto [\sin(k_L x + \varphi)\epsilon_+ - \sin(k_L x - \varphi)\epsilon_-]$, where $\epsilon_\pm = \hat{e}_2 \pm i\hat{e}_3$, $k_L = 2\pi/\lambda$ the laser wave vector and φ is the polarization angle. The resulting electric field with laser frequency ω is therefore,

$$\mathbf{E}(x,t) = E_+(x)\epsilon_+ e^{-i\omega t} + E_-(x)\epsilon_- e^{i\omega t}, \tag{2.1}$$

here $\mathbf{E}_\pm(x) = \sin(k_L x \pm \varphi)$, with angle φ making it possible to selectively move the nodes of both standing waves. Moreover, a single stationary periodic field can be produced [Huckans et al 2009] out of these using parallel polarization, i.e. $\varphi = 0$, which is the concept behind many of the general optical lattice potentials.

2.1.1 Interaction Hamiltonian

Assuming that the electric field generated is purely classical which interacts with a quantized atom in the conservative manner, i.e. far off frequency detuning from inter-atomic transitions. The coupling between field intensity and the induced dipole moment holds a semi-classical description in the interaction picture. The complete Hamiltonian reads,

$$\hat{H} = \hat{H}_{cm} + \hat{H}_A + \hat{H}_I = \frac{p^2}{2m} + \frac{1}{2}\hbar\omega_o\sigma_z - \hat{\mathbf{d}}.\mathbf{E}(x,t), \tag{2.2}$$

where, $\hat{H}_{cm}$ counts for the intrinsic center of mass kinetic energy of the atom. And the second term consists of the internal degrees of freedom of the atom, which in our

case supposed to have two levels, for simplicity. The internal states are denoted by $|g\rangle$ and $|e\rangle$ which defines the Pauli matrix as $\sigma_z = |e\rangle\langle e| - |g\rangle\langle g|$. The last term in above equation corresponds to interaction Hamiltonian which needs further solution. Using completeness relation, we write

$$\hat{H}_I = -[\langle e|\hat{\mathbf{d}}.\mathbf{E}(x,t)|g\rangle\sigma_+ + \langle g|\hat{\mathbf{d}}.\mathbf{E}(x,t)|e\rangle\sigma_-], \tag{2.3}$$

here $\sigma_\pm$ represents the atomic transition operators and $\hat{d}$ the dipole moment operator which causes the diagonal terms to drop off. Above equation follows

$$\hat{H}_I = -[\ \boldsymbol{\mu_{eg}} \cdot \boldsymbol{\epsilon}_+ E(x) e^{-i\omega t}\sigma_+ + \boldsymbol{\mu}^*_{\boldsymbol{eg}} \cdot \boldsymbol{\epsilon}_- E(x) e^{i\omega t}\sigma_-], \tag{2.4}$$

where μ_{eg} denotes the off diagonal dipole matrix element defining the field dependent Rabi frequency

$$\Omega(x) = \frac{\boldsymbol{\mu_{eg}} \cdot \boldsymbol{\epsilon}_\pm E(x)}{\hbar}. \tag{2.5}$$

Now, for a stationary sinusoidal field with parallel polarization,

$$\hat{H}_I = -\hbar\Omega_o \sin(k_L x) e^{-i\omega t}\sigma_+ + H.c\ . \tag{2.6}$$

A convenient option is to solve the time independent Hamiltonian proceeding from the rotating frame of the laser. Such an approximation holds good in the realm of far off detuning (Δ) between field and transition frequency, where the counter rotating phases $\sigma_+ e^{-i\omega t}$ and $\sigma_- e^{i\omega t}$ are ignored by time averaging [Louden 1983]. Hence the effective Hamiltonian of a two level atom coupled to a stationary wave ends to,

$$\hat{H} = \frac{p^2}{2m} - \frac{\hbar\Delta}{2}\sigma_z - \hbar\Omega_o \sin(k_L x) + H.c\ . \tag{2.7}$$

For a segregate treatment of overall atomic transport irrespective of the internal degrees of freedom, we take the ansatz

$$|\Psi(x,t)\rangle = \Psi_g(x,t)|g\rangle + \Psi_e(x,t)e^{-i\omega t}|e\rangle\ . \tag{2.8}$$

Solving Schrodinger equation for effective Hamiltonian using above ansatz, yields a pair of coupled differential equations,

$$\begin{aligned} i\hbar\frac{\partial\Psi_g}{\partial t} &= -\frac{\hbar^2}{2m}\frac{\partial^2\Psi_g}{\partial x^2} - \hbar\Omega_o \sin(k_L x)\Psi_e\ , \\ i\hbar\frac{\partial\Psi_e}{\partial t} &= -\frac{\hbar^2}{2m}\frac{\partial^2\Psi_e}{\partial x^2} - \frac{\hbar\Omega}{2}\Psi_e - \hbar\Omega_o \sin(k_L x)\Psi_g\ . \end{aligned} \tag{2.9}$$

With properly detuned laser beams the inter atomic transitions can be neglected [Graham et al 1992]. Such a conservative interaction induces a shift in the potential energy of both internal states, known as the AC Stark shift, which can be calculated making use of perturbation theory. Second order corrections to the energy bring about the effective potential faced by atoms. That is,

$$V(x) = \pm\frac{|\langle e|\hat{H}|g\rangle|^2}{\hbar\Delta} = \frac{\hbar\Omega(x)^2}{\Delta} \; . \tag{2.10}$$

Moreover, at a fairly large detuning the excited state is very less probable [Saif 2005a]. Thus it can be adiabatically ignored. In such a scenario the atom field dynamics are completely dictated by the ground state probability coefficients which effectively describe the system's evolution,

$$i\hbar\frac{\partial\Psi_g}{\partial t} = -\frac{\hbar^2}{2m}\frac{\partial^2\Psi_g}{\partial x^2} + \frac{\hbar\Omega_o^2}{\Delta}\sin(k_L x)\Psi_e \; . \tag{2.11}$$

Taking $V_o = \hbar\Omega_o^2/\Delta$, defines the lattice depth which is adjustable through the detuning $\Delta = \omega - \omega_o$. Furthermore, for blue detuning ($\Delta > 0$) atoms gain subsistance towards minimal intensity nodes. Whilst for red detuned ($\Delta < 0$) laser beams the direction is towards maximal nodes of standing wave. The effective Hamiltonian of an atom in its ground state is given as,

$$\hat{H} = \frac{p^2}{2m} + V_o\sin^2(k_L x) \; . \tag{2.12}$$

Such an assembly of optical components is called optical lattice. The generated periodic potential governs the dynamics of loaded gas atoms. Depending upon the potential depth the trapped entities hop between periodic lattice sites. This bring about plenty of novel phenomena studied in solid state physics. In respect of this close resemblance, optical lattices are considered as a self assembled "test bed" for most of the quantum theories.

The intrinsic hopping attached to optical lattice also causes loss of atoms. That's why additional trapping potentials are inevitable. Also some particular experiments mostly require strictly localized atoms with large decay times. A parabolic trap mostly serves for the purpose, whose effects are at the heart of this chapter and will be discussed shortly.

2.1.2 Central Equation and Bloch's Theorem

Optical lattice complements the conventional crystal structures by giving access to perfectly pure crystals where the potential is seen by the atoms instead of electrons. A breif study of the formalisms ascribed to solid state crystals is therefore necessary, to describe the main characteristics of cold atoms in periodic potentials. In this context we gently follow the work of Morsch [Morsch and Oberthaler 2006] and similarly proceed from the one-dimensional study of periodic potential, which can simply be extended to higher dimensions. The stationary Schrodinger equation of an atom in potential $V(x)$ reads,

$$-\frac{\hbar^2}{2m}\frac{\partial^2\psi(x)}{\partial x^2} + V(x)\psi(x) = E\psi(x)\ . \tag{2.13}$$

For the particular case of $V(x) = 0$ the eigenstates are familiar plane waves. While for the celebrated case of periodic optical potential, i.e. $V(x + md) = V(x)$ with spacing d, the solution follows from the famous *Bloch's Theorem*,

$$\psi_k^l(x) = e^{ikx}u_k^l(x), \tag{2.14}$$

where k represents the usual crystal momentum and $u_k^l(x)$ is the periodic potential whose period commensurate with that of the lattice. In turn giving rise to periodic Bloch states of same period. Using Fourier series

$$\psi_k^l(x) = e^{ikx}\sum_q C^l(k,q)e^{iqx}. \tag{2.15}$$

These are Bloch states modulated in the rythm of periodic potential [Bloch 1929]. The existence of periodic optical lattice maps the plane waves onto the Bloch states. Thats why Bloch states are totally de-localized. Also, the forbidden energy zones elicits in the presence of periodic potential as a consequence of matter wave diffractions, which is the concept behind the formation of so called Band structures.

Expanding $V(x)$ in terms of its Fourier series,

$$V(x) = \sum_n V_n\ e^{iKx}, \tag{2.16}$$

here $K = 2\pi n/d$, representing the primitive reciprocal lattice vector. Using the above expansion and Eq. 2.13 with the Bloch wavefunctions, we get the difference equation

$$[(q+k)^2 - E]C^l(k,q) + \sum_n V_n\, C^l(k, q-K_n) = 0\ , \tag{2.17}$$

known as the central equation. This is a matrix equation, which is particularly diagonal, where the coefficients are coupled depending upon the k values in first Brillouin zone. The eigenvalues obtained from this equation are the energy values E_k^l for each k which contribute to band formation, labelled as Band index l.

In next subsection we calculate the Hamiltonian matrix for the sinusoidal optical potential and see how different energy bands and lattice depth contribute to Bloch states.

2.1.3 The Sinusoid Potential

For an atom moving in the one dimensional optical sinusoid, similar to that of an optical lattice potential produced earlier, Eq. 2.16 takes the form

$$V(x) = \upsilon_o E_r\ \sin^2(k_L x) = \frac{\upsilon_o E_r}{4}[2 - e^{2ik_L x} - e^{-2ik_L x}]\ , \tag{2.18}$$

where, $E_r = \hbar k_L^2/2m$ is the relevant energy scale. Clearly, only three terms sustains in the Fourier sum with $n = 0, \pm 1$ relating to first Brillouin zone in the scaled units. The central equation for this sinusoidal potential follows,

$$[(q+k')^2 + \frac{\upsilon_o}{2} - E^{'}]C^l(k,q) + \frac{\upsilon_o}{4}[C^l(k,q-1) + C^l(k,q+1)] = 0\ , \tag{2.19}$$

reduced matrix representation of above equation is given as,

$$\begin{bmatrix} \frac{1}{2}\upsilon_o + 4(k'-2)^2 - E_k^l & -\frac{1}{4}\upsilon_o & 0 & 0 & 0 \\ -\frac{1}{4}\upsilon_o & \frac{1}{2}\upsilon_o + 4(k'-1)^2 - E_k^l & -\frac{1}{4}\upsilon_o & 0 & 0 \\ 0 & -\frac{1}{4}\upsilon_o & \frac{1}{2}\upsilon_o + 4(k')^2 - E_k^l & -\frac{1}{4}\upsilon_o & 0 \\ 0 & 0 & -\frac{1}{4}\upsilon_o & \frac{1}{2}\upsilon_o + 4(k'-1)^2 - E_k^l & -\frac{1}{4}\upsilon_o \\ 0 & 0 & 0 & -\frac{1}{4}\upsilon_o & \frac{1}{2}\upsilon_o + 4(k'-2)^2 - E_k^l \end{bmatrix} \begin{bmatrix} C^l(-2,k) \\ C^l(-1,k) \\ C^l(0,k) \\ C^l(-1,k) \\ C^l(-2,k) \end{bmatrix} = 0,$$

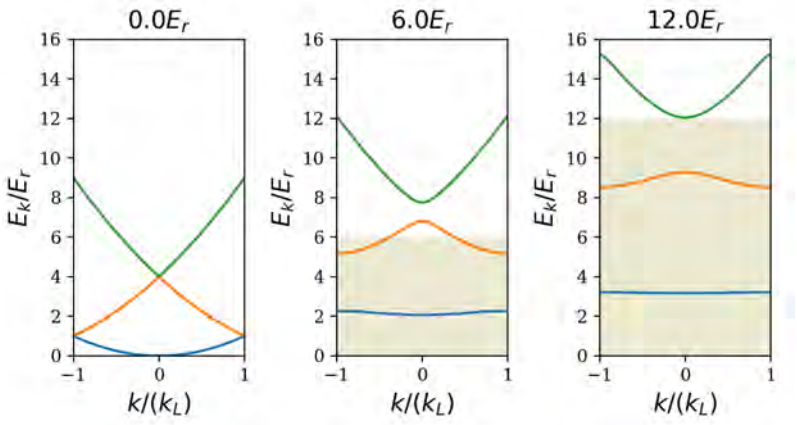

Figure 2.2: Emergence of energy bands in the presence of optical lattice potential. Band gap increases as soon as potential depth is raised which is marked by shaded regions.

where the infinite matrix relation is reduced to lower orders at a suitable truncation. Above equation can now easily be diagonilized to obtain the eigenvalues E_k^l with eigen vectors exclusively determining, $C^l(k,q)$, the Bloch coefficients. In the numerical simulations we have truncated the infinite set at $|q| \leq 5$, which satisfies the condition that, for efficient solutions, the truncation to q should be greater than the band index. The whole computation recipe is performed using basic *Python* libraries where we have preferred Qutip for diagonalizing above matrix.

The band structure obtained is shown in Fig. 2.2, as a function crystal momentum k and lattice depth V_o, which depicts origin of energy bands as soon as the optical lattice intervenes. Without an optical lattice the solution follows the usual free particle dispersion curve. The instant periodic potential is turned on, the curves in the reduced zone scheme begin to segregate, where the band gap grows with lattice depth.

This is the band structure of an optical lattice, mostly connected to electronic motion in solid state crytals. Achieving such a same degree of quantumness at a milionth scale with genuine control is actually quite remarkable. Now cold atoms can be manipulated in these quantized energy bands, adduce to the experiment at Aarhus [Pedersen et al 2013].

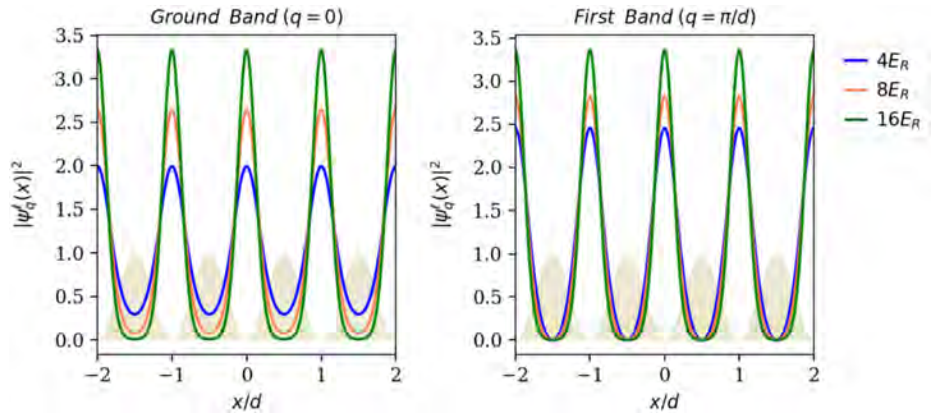

Figure 2.3: Eigenstates of 1D optical lattice computed by exact diagonalization of Eq. 2.19 for $l = 0$ (left) and $l = 1$ (right) at different potential depths. The states obtained are normalized to one over each lattice site. The shaded area is shown to highlight the presence of optical potential.

Spatially periodic Bloch states are also traced using the Bloch coefficients obtained in previous procedure. Fig. 2.3 shows the result for couple of initial bands, at various potential depths. The probability density is being plotted as a function of scaled position. The results show an increase in the weight over each potential minima with increase in potential depth.

2.1.4 Wannier States

An alternate decription holds in terms of spatially localized Wannier functions which serves equally good in the description and commputations of band structure. Bloch functions are fully extended over the whole lattice with a delocalized plane wave envelope, i.e. e^{ikx}. A localized wave packet can be forged by summing over all the k Bloch states in the Brillouin zone,

$$\omega^{\ell}(x - x_j) = \frac{1}{\sqrt{N}} \sum_{Bz} \psi_k^l(x) e^{-ikx_j}. \tag{2.20}$$

These alternative basis that turns out to be appropriate to describe inter-particle hopping amongst different lattice sites, are called the Wannier states [Wannier 1937]. They are simply connected to Bloch states by a Fourier transform, with proper normalization over the first Brillouin zone. To simplify the notation, Wannier functions

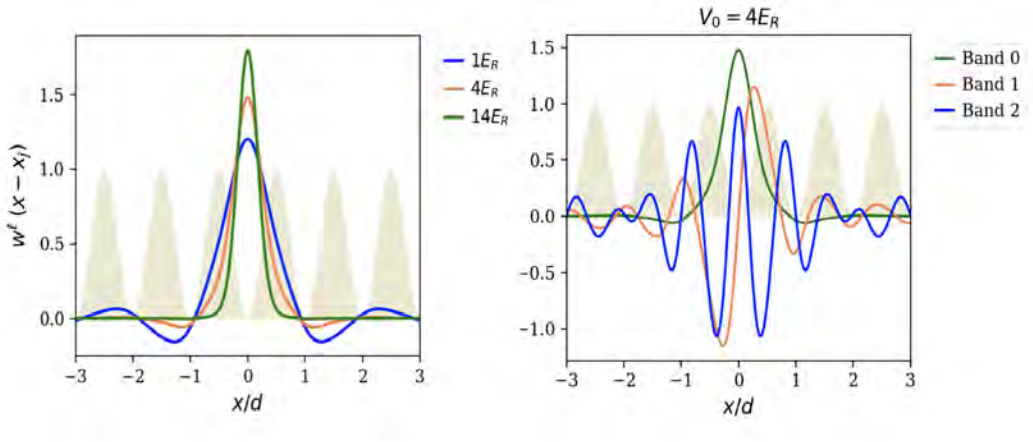

Figure 2.4: Localized Wannier states at the center of lattice, i.e. $x_j = 0$. Variation with the potential depth in the ground band is shown (left), along with higher bands (right) at a fixed value of potential. The shaded area is shown to highlight the presence of optical potential.

can be written in the Dirac formalism,

$$|n, l\rangle = \frac{1}{\sqrt{N}} \sum_k |k, l\rangle e^{-ikx}. \tag{2.21}$$

Fig. 2.4 depicts the localization effect of Wannier states which increases by rise in lattice depths. The states become more and more localized by increasing V_o (left), reaching a maximum localization bound. The limit can be found making use of the standard deviation formula. The plot on the right shows three lowest wannier orbitals where the localization of the states diminishes for higher bands at a constant optical lattice amplitude. The states engineered are more workable in describing the hopping properties of periodic lattices [Marzari et al 2012]. The added convenience can be seen in the upcoming single band treatments.

2.2 Quasi 1D Optical Lattices

The minimalistic experimental setup of two beam architecture produces optical lattice with a spacing d given by half of the laser wavelength [Morsch and Oberthaler 2006]. With proper detuning optical lasers automatically provide centeral confinement in the radial direction. Although this confinement doesn't last long for the specific case

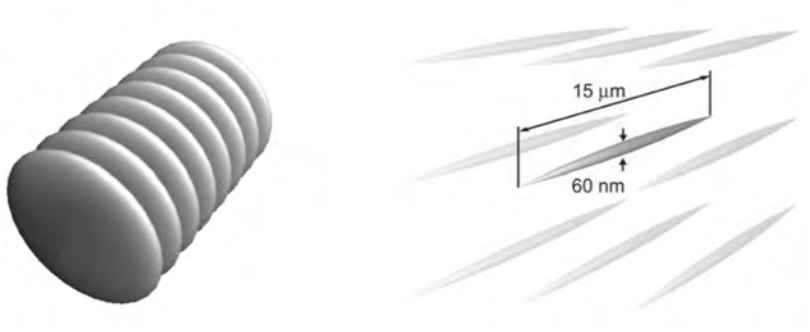

Figure 2.5: Surface of constant potentials generated in the minimalistic two-beam configuration (left) and arrays of modulated optical tubes (right) [Paredes et al 2004] generated with a six beam setup. In the later an external, weak modulation across the tubes might be necessary to attain arrays of truly 1D optical lattices.

of one dimensional architectures. Precisely for a blue detuned laser setup the decay time is very sharp. Thus it requires external halting potential in addition.

Particular two beam setup with red detuning form a pancake like structure of fixed potential, as shown on the left of Fig. 2.5. Therefore, a weaker confinement may halt the transverse modes in a non-trivial fashion. A weak parabolic potential mostly serves for the purpose and this causes the realization of quasi 1D optical lattices, which is one of the turning points towards parabolic optical lattices.

There also exists a truly 1D optical lattice which is well known by the name of modulated optical tubes. This is a typical six beam setup analogous to a 3D optical molasses where the four beams confine the atoms into transverse structures. While the left two periodically modulate the elongated tubes with a weak driving. The lattice so formed is shown to the right of Fig. 2.5.

Whether it is a modulated optical tube or a quasi 1D optical lattice, there pertains an intrinsic tunnelling of atoms, accredited to the quantumness at lower temperatures. Ultracold atoms stored in an optical lattice are not static and will continuously tunnel from one lattice site to the other. Lets analyse in the next section what we can do to counterfeit this hopping effect.

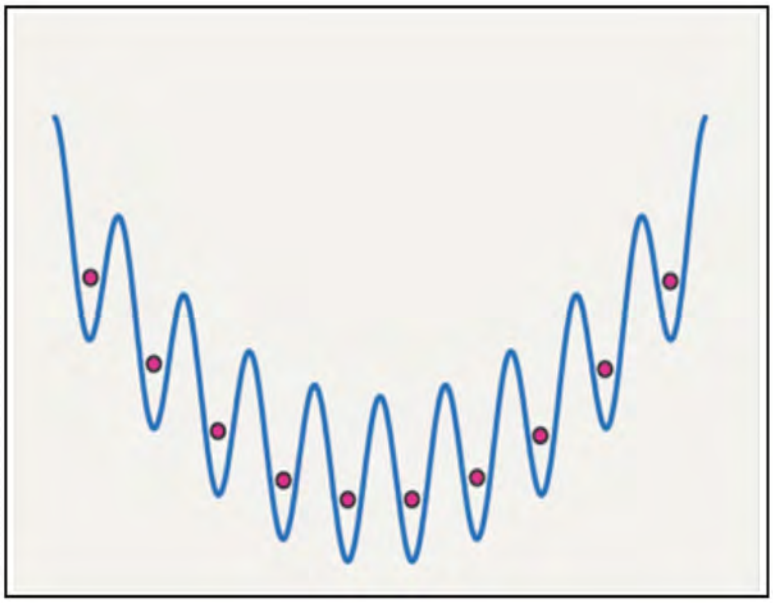

Figure 2.6: 1D Parabolic Optical Latice

2.3 Role of Parabolic Confinement

Keeping an eye on the context of all above inherent escaping problems, an external parabolic potential is indispensable. The potential might be optical or magnetic but the special part is it must be slow harmonic. And the system so formed in the combined potential of an optical lattice and a parabolic trap is called parabolic optical lattice. The Hamiltonian is,

$$H = \frac{p^2}{2m} + V_o \sin^2 (k_L x) + \frac{1}{2} m \omega_T^2 x^2 \ , \tag{2.22}$$

where ω_T is the frequency of the trap. Above equation is a prototype of a harmonic oscillator defined on a lattice and greatly resembles to Bloch electrons in effect of a quadrupole potential. In the absence of last term the system is periodic in space whereas, the presence of halting potential makes the system symmetric in space. Hence a general solution is not yet available and the presence of additional trap substantially redefines the system dynamics, which will be discerned in the upcoming chapters. For now we set the foundations for that detailed treatment.

2.4 Tight Binding Description

The usual Wannier picture describe the most coveted positions of atoms. The maximally locaized Wannier states delineate the whole weight of atoms around fixed lattice sites. Thus ultracold atoms can be considered as an approximate harmonic oscillator at each potential minima. However, their will be a finite tunneling rate due to wave function overlaps. We only consider tunneling between contiguous lattice sites and restrict ourself to a single Wannier band. A combination of such terms is mostly known by the name of tight binding approximation. Now, as the Wannier basis $|n, l>$ complete an orthonormal set so they can be written in terms of field operators,

$$\hat{\psi} = \sum_n |n, l\rangle \hat{a}_n \qquad \Rightarrow \qquad \hat{a}_n = \langle n, l|\hat{\psi} \ , \tag{2.23}$$

Here, $\hat{\psi}$ is an operator in the second quantization guiss where $\hat{a}_i^\dagger$ creates a particle on the ith site and $\hat{a}_i$ obliterates. The second quantized Hamiltonian follows,

$$H = \hat{\psi}^\dagger \hat{H} \hat{\psi} \ , \tag{2.24}$$

$$H = \sum_{n,m} \hat{a}_n^\dagger \langle n, l|\hat{H}_o + \hat{H}_T|m, l\rangle \hat{a}_m \ , \tag{2.25}$$

where $\hat{H}_T$ denote the trap Hamiltonian and H_o the remaining terms of Eq. 2.22. Also to simplify the notation fixed band indices in $\hat{a}$ ($\hat{a}^\dagger$) are suppressed from the start,

$$H = -J \sum_{n,m} \hat{a^\dagger}_n \hat{a}_m + \sum_{n,m} \hat{a^\dagger}_n \hat{a}_m \varepsilon_{nm} \ . \tag{2.26}$$

Equation introduces two important components of the model, i.e. tunneling parameter $J = -\langle n|\hat{H}_o|m\rangle$ and single atom energy $\varepsilon_{nm} = \langle n|\hat{H}_T|m\rangle = \delta_{mn} \int V_T(x)|\omega_n(x)|^2 dx$ $\approx$ $V_T(x_n) \approx d^2 n^2$, defined in the most compact form. Above equation follows

$$H = -\frac{J}{2} \sum_n (\hat{a}_n^\dagger \hat{a}_{n+1} + \hat{a}_{n+1}^\dagger \hat{a}_n) + \sum_n \hat{a}_n^\dagger \hat{a}_n \varepsilon_n \ , \tag{2.27}$$

where we have used $m = n+1$ in regard of the nearest neighbouring coupling argument of tight binding description. Substituting the single atom energy gives

$$H = -\frac{J}{2} \sum_n (\hat{a}_n^\dagger \hat{a}_{n+1} + \hat{a}_{n+1}^\dagger \hat{a}_n) + \frac{1}{2} m\omega_\tau^2 d^2 \sum_n n^2 \hat{a}_n^\dagger \hat{a}_n \ , \tag{2.28}$$

which is the tight binding Hamiltonian of parabolic optical lattice, written in terms of field creation annihilation operators. Reverse engineering by making use of Eq. 2.23 in above equation give rise to an alternate representation given by

$$\hat{H} = -\frac{J}{2}\sum_{n}(|n\rangle\langle n+1|+|n+1\rangle\langle n|) + \frac{1}{2}m\omega_{\tau}^{2}d^{2}\sum_{n} n^{2}|n\rangle\langle n| \; . \tag{2.29}$$

That is the exact form of tight binding hamiltonian in Wannier picture, which substantially simplifies the analytical description. In addition, numerical efforts are also reduced bringing much easier and efficient computations. As will be seen in the results of upcoming chapters.

2.4.1 First Band Tunneling Parameter

As introduced in the previous section, tunneling parameter is an important quantity in dictating overall atomic motion in optical lattices. Here we derive an approximate relation for its relation with the optical potential depth. Proceeding as

$$J = -\langle n,l|\hat{H}_{o}|m,l\rangle = -\frac{1}{\sqrt{N}}\, e^{ikx}\, \langle k',l|\frac{p^{2}}{2m} + V_{o}\sin^{2}(kx)|k,l\rangle,$$

$$J = -\frac{1}{\sqrt{N}}\sum_{k} E_{k}^{l}\, e^{ikx}. \tag{2.30}$$

The energy band width Δ^{l} at $V_{o} >> Er$ holds the asymptotic expression [Ayub et al 2009]

$$\Delta^{l} = \frac{2^{3l+4}}{l!\,\sqrt{\pi}}\left(\frac{V_{o}}{E_{r}}\right)^{\frac{l}{2}+\frac{3}{4}} e^{-2\sqrt{\frac{V_{o}}{E_{r}}}}\left[1 - \frac{6l^{2}+14l+7}{16}\sqrt{\frac{E_{r}}{V_{o}}} + O\left(\frac{E_{r}}{V_{o}}\right)\right]. \tag{2.31}$$

As we know in the absence of parabolic potential the Bloch states form band structure of width $\Delta^{l} = 4J$ around origin. Therefore, from above solution at $l = 0$ we write

$$J = \frac{4}{\sqrt{\pi}}(s)^{\frac{3}{4}}e^{-2\sqrt{s}} \; , \tag{2.32}$$

that is the relation between tunneling parameter and the lattice amplitude. Hence the lattice hopping can be tuned from outside which elicits beautiful dynamical features with accurate control.

The Wannier functions considered till now are free from inter-atomic interactions. Such single-particle treatment holds good in the situation where a single ultracold atom attains a particular localized optical lattice site. Although the work can be extended to Hubbard model or two band tight binding model where higher order coupling effects are also analysed. The forgoing examination is restrained to non-interacting ultracold Bosons, leaving non-linear effects a future endeavour.

Chapter 3

Single Band Approximation

The addition of an external potential breaks the uniformity of periodic lattices making it symmetric in space. The nonlinear term intricates the dynamics, even for single atoms, reducing the feasibility of a comprehensive analytical solution. However, the quasimomentum representation allows single atom evolutions to be determined exactly, the same method prove to be inadequate when atom-atom interactions are involved. Luckily, there exists an approximation which effectively aids in simplifying the model Hamiltonian, still preserving the accuracy. That is well known by the name of single band approximation [Biao et al 2012]. The model is more generic in approach than the previously discussed tight binding model. Pre-determined Wannier states of the lowest Bloch band are exploited to map the system on a lattice model such as Hubbard model, which considerably rationalize the inbred dynamics. This chapter introduces Bloch oscillations and mainly address the single band dynamics of parabolic optical lattice, also covering the semi-classical depiction introduced by us.

3.1 Optical Lattice Ground Band Energy

In the Wannier representation, the time dependent wavefunction of a state in the lowest Bloch band can be written as

$$\psi(x,t) = \sum_n \phi_n(t)\psi_n(x), \tag{3.1}$$

here, $\psi_j(x) = \psi_j(x - nd)$ is the ground state of n^{th} lattice site and

$$\phi_n(x) = \sqrt{c_n(t)}e^{-i\varphi_n t}, \tag{3.2}$$

is an imaginary function describing the complex amplituds, $\sqrt{c_n}$, and the phases, φ_n, related to the wavefunction on n^{th} site. The respective coefficients satisfy the discrete nonlinear Schrodinger equation

$$i\hbar\frac{\partial\phi_n}{\partial t} = -J(\phi_{n-1} + \phi_{n+1}), \tag{3.3}$$

which has the solution in terms of Bloch states with the garnishing plane waves replaced by complex functions $\phi_n(t) = e^{i(nkd-Et/\hbar)}$. In this scenario the phase difference between contiguous sites is constant through out the lattice, i.e. $\Delta\varphi = \phi_{n+1} - \phi_n = kd$ and depends upon momentum k. For a sufficiently deep lattice, using this Bloch ansatz, above equation has a solution which gives an analytical expression for the energy of lowest Bloch band [Ayub 2012]

$$E_o(k) = \epsilon_o - 2J\cos(kd)\ , \tag{3.4}$$

where ϵ_o denote a constant energy, determined by potential depth. This is the ground band energy of an optical lattice without any external potential. It is worth mentioning that the Wannier states taken here are free from interaction effects and the interaction terms are calculated separately even in the single band approximations.

3.2 Tilted Optical Lattice

To give a short introduction of Bloch oscillations we give a brief review of the tilted optical lattice that is formed by the optical lattice in the presence of a constant linear force. The potential generated is tilted with a uniform slope, also called a washboard potential. The Hamiltonian corresponding to the tilted lattice is then

$$H = \frac{p^2}{2m} + V_o\sin^2(k_L x) + Fx\ , \tag{3.5}$$

where F represents the static force. The corresponding spectrum is quantized and well known by the name of Wannier-Stark ladders. The reason behind the name is the appearance of equi-spaced localized set of energies in each well. And the word Stark is ascribed owing to the Stark shift induced by external forcing field. While Wannier was the first to describe the phenomenon [Wannier 1960], followed by a long debate on the topic. The work history is well summarized in [Bouchard and Luban 1995; Krieger and Iafrate. 1986].

Figure 3.1: Atomic motion in a tilted optical potential. The constant linear force submerged upon the lattice yielding uniform tilt.

The dynamics generated in effect of static tilt are totally non-intuitive. Classically, we expect an accelerated motion towards infinity. But one observes coherent oscillations with period

$$T_B = \frac{2\pi\hbar}{Fd} \, . \tag{3.6}$$

The simplistic tilted band picture, which goes back to Zener's celebrated paper [Zener 1934], foregrounded the dynamical features of the system. An alternative description appeared in terms of "acceleration theorem" which also uses field-free Bloch bands. The wavepacket accelerates with a quasimomentum varying linearly in time $k_t = k_o + Ft/\hbar$, until Brillouin zone sweeps. The time zone boundary is reached Bragg reflection occurs, it turns back in real space and then it oscillates. These are the Bloch oscillations tilted optical lattice known for. The phenomenon will be discussed in detail soon.

3.2.1 Lattice Acceleration

Lets move to the acceleration frame which is the same as the interaction representation of tilted potentials. Transforming the Schrodinger equation with the new wavefunctions

$$\tilde{\psi}(x) = \exp\left(-\frac{i}{\hbar}Ftx\right)\psi(x) \, , \tag{3.7}$$

the tilted optical lattice Hamiltonian Eq. 3.5, transforms to the new Hamiltonian, where only the single particle terms vary from their original version. The transfor-

mation thus leads the following form

$$\tilde{H} = \frac{(p + Ft)^2}{2m} + V_o \sin^2(k_L x) \ , \tag{3.8}$$

which results in the emergence of a time dependent vector potential and the linear potential is gauged away [Saif and Watanabe 2019]. The underneath algebra follows $x' = x + Ft^2/2m$, which implies $p' = p - Ft$, it is seen that an effective linear slope Fx is congruent to an acceleration F/m of the optical lattice.

3.2.2 Bloch Oscillations and Landau-Zener Tunneling

The dynamics of a Bloch particle, i.e a quantum particle moving in a periodic potential with energy as a function of quasimomentum and an unavoidable energy gap between lowest bands, bring about a totally non-trivial system response to an external linear static force.

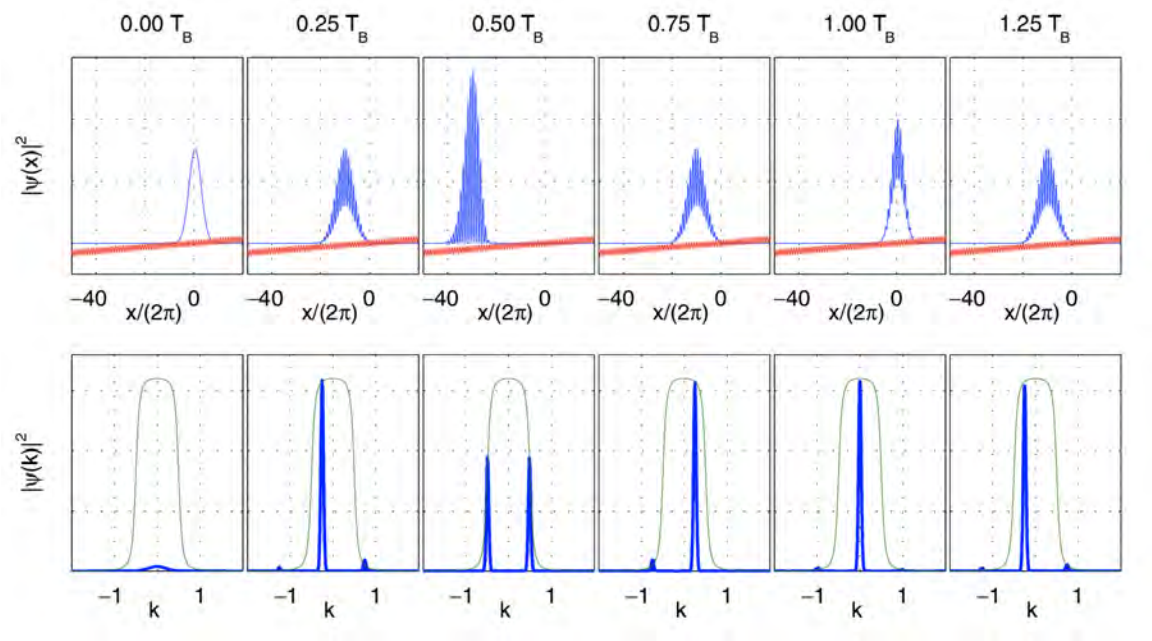

Figure 3.2: Schematic Illustration of Bloch oscillation [Hartmann et al 2004]. Shown is the squared amplitude of wavefunction both in sptaial and momentum representation.

Considering the Hamiltonian 3.8, garnished by an additional linear potential gauged away. The adiabatic spectrum (i.e. for static vector potentials) commensurate with

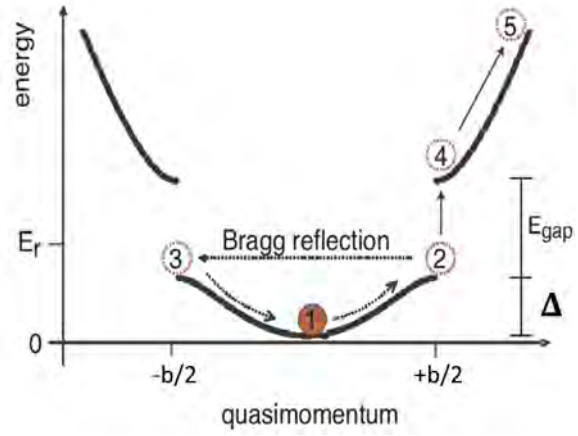

Figure 3.3: Band structure depiction of Bloch oscillations and Landau-Zener tunneling in the extended zone representation [Modugno et al 2004], where position (1) marks the quantum particle placed in the lowest Bloch band.

that of H_o. But for a time dependent vector potential the quasimomentem is distributed linearly in time $k(t) = k_o + Ft/\hbar$. Under the assumption of a moderate static force that does not cause the first two bands to overlap, $Fd << \Delta$, the energy of a wavepacket initially generated in the ground band (1 in Fig. 3.3) , adiabatically evolves as $E_o(k + Ft/\hbar)$ till it reaches the Brillouin zone edges. As soon as the zone boundary is reached (marked position 2) the particle experiences Bragg reflection. That is the momentum reverts (marked position 3) and the wavepacket changes its direction, returning to its initial outset and the cycle continuous with the Bloch frequency $\omega_B = Fd/\hbar$. This subsequent modulation of the particle mean momentum and position is called Bloch oscillations [Hartmann et al 2004].

Another enrichment to the dynamics which effectively hinders the Bloch oscillations, rather can be sheded, is the Landau-Zener tunneling. Band picture is again involved here and some part of the wavepacket reaches higher bands owing to the quantumness (tunneling) at smaller band gaps [Holthaus 2000]. Band gap reduces by an increased static tilt and the effect of Bragg diffraction pertains over Bragg reflection. The whole assembly is schematically depicted in Fig. 3.3, where the second band occupation (marked position 4) is also shown. The tunnelled fraction accelerates at higher energies performing roller coaster cascaded motion until it relegates. The dynamics

are closer to classically expected transport but in the root cause again quantumness involved. It is actually really very interesting that in Bloch oscillations classical transport was suppressed by quantum mechanics. The origin of same classicality from quantum tunnelling phenomenon is quite amazing.

Bloch oscillations of a particle is shown in Fig. 3.2 in the single band approximation where all the Landau-Zener tunnelling is redundant. We think the illustrations serves well in understanding these fancy quantum phenomena. The parametric values used are given in the tabular form.

Table 3.1: Parametric values for Bloch oscillation simmulation.

$s = V_o/E_r$	F	$\hbar_{eff}$
1.4	0.005	3.3806

As a brief analytical description we would like to present some analysis from the work of Holthaus [Holthaus 2000], which shows the transition rate to higher band to be given by

$$T = \frac{1}{T_B}|T|^2 \,, \tag{3.9}$$

which measures the fractional loss of ground band population to first band. It also well determines the upper bounds of maximum magnitudes of the static force,

$$[Fd/E_r]_{max} \approx \frac{V_o}{4E_r} \,, \tag{3.10}$$

when calculated by the Landau-Zener relation for the tunnelling probability $|T|^2$ [Zener 1932],

$$|T|^2 \approx \exp\left(\frac{\pi^2\Delta}{8Fd/E_r}\right). \tag{3.11}$$

In regard of the above defined limits we confine ourself to the interval $[0, F_{max}]$, in the single band approximation, with F_{max} defined by the Eq. 3.10. Hence, under these suppositions, projection of the Hamiltonian Eq. 3.8 onto the ground band produces the following form, in quasi-momentum representation [Grecchi and Sacchetti 1995],

$$H(k) = E_o(k + Ft/\hbar) \,, \tag{3.12}$$

with no coupling to first band.

3.3 Mean Atomic Motion

Lets find out how the single particle observables evolve during one time period. The time evolution of canonically conjugate variables is governed by the Heisenberg equations of motion

$$\frac{dk}{dt} = \frac{i}{\hbar}[H(k), k] = \frac{i}{\hbar}[E_o(k + Ft/\hbar), k] = 0 \ , \tag{3.13}$$

$$\frac{dx}{dt} = \frac{i}{\hbar}[H(k), x] = \frac{i}{\hbar}[E_o(k + Ft/\hbar), -i\frac{\partial}{\partial k}] = \frac{1}{\hbar}\frac{\partial E_o(k + Ft/\hbar)}{\partial k} \ . \tag{3.14}$$

The first equation leads to conservation of the quasimomentum vector which remains constant $k = k_o$ in the accelerating frame. Whereas, the solution of second equation contribute to periodic time dependence of the momentum operator besides the periodicity of $E_o(k)$.

Now, for an initial state which can be decomposed into Bloch basis,

$$\psi(x, t_o) = \sum_{Bz} f_k(t_0)\psi_k(x) \ . \tag{3.15}$$

The mean atomic observables follow

$$\langle p(t)\rangle = \sum_{Bz} |f_k(t_o)|^2 \ \frac{\partial E_o(k + Ft/\hbar)}{\partial k} \ , \tag{3.16}$$

$$\langle x(t)\rangle = \left\langle \int_{t_o}^{t} p(t')dt' \right\rangle = x_o + \frac{1}{F}\sum_{Bz} |f_k(t_o)|^2 [E_o(k + Ft/\hbar) - E_o(k)]. \tag{3.17}$$

Using Eq. 3.4 we write

$$\langle p(t)\rangle = 2dJ \sum_{Bz} |f_k(t_o)|^2 \ \sin(kd + \omega_B t)k, \tag{3.18}$$

$$\langle x(t)\rangle = x_o - \frac{2J}{Fd} \sum_{Bz} |f_k(t_o)|^2 \ [\cos(kd + \omega_B t) - \cos(kd)]. \tag{3.19}$$

Above equation ascertains the presence of Bloch oscillations with amplitude $2J/Fd$ and highlights a couple of evolutionary instances. That is oscillation amplitude attains a maximum for sharply localized quasimomentum distributions $f_k(t_o) = \delta_{k,k_o}$. Thus a narrow quasimomentum width is prime for observing Bloch oscillations in real space.

3.4 Effects due to Parabolic Confinement

The dispersion relation of a particle in the optical lattice effected by a quadratic forcing is given by

$$H(k) = -J\cos(kd) + F_1 x^2, \tag{3.20}$$

where F_1 quantifies the relative strength and is used to represent the notion of force originating from a parabolic trap. With this the mean atomic observables derived above, in this case, leads to

$$\hbar\dot{k} = -\frac{\partial E(k)}{\partial x} = -2F_1 x, \tag{3.21}$$

and the group velocity follows,

$$\dot{x} = \frac{\partial E(k)}{\hbar \partial k} = \frac{Jd}{\hbar}\sin kd\ . \tag{3.22}$$

The above coupled equations results in an oscillator equation [Saif and Watanabe 2019]

$$\hbar\ddot{k}(t) = -\frac{2dJF_1}{\hbar}\sin(kd)\ , \tag{3.23}$$

which can be solved considering the time dependent ansatz $K(t) = k\sin(\eta t)$, where η is an unknown frequency. Substituting the ansatz above equation reduces to the equality

$$\begin{aligned} k\eta^2\sin(\eta t) &= \frac{2dJF_1}{\hbar^2} sin(kd\sin(\eta t)) \\ &= \frac{2dJF_1}{\hbar^2}\sum_{n=0}^{\infty} J_{2n+1}(kd)\sin[(2n+1)\eta t]\ . \end{aligned} \tag{3.24}$$

On comparing the coefficients of $\sin(\eta t)$ on both sides, we get

$$\eta^2 = \frac{2J\Omega}{\hbar^2}J_1(kd)\ , \tag{3.25}$$

where we have introduced the parabolicity $\Omega = F_1 d$, which mainly depends upon the trap strength F_1. Clearly, the frequency of the oscillator depends upon quasi-momentum k. For k approaching to zero, we get the well known dipole oscillations frequency

$$\eta_o = \omega_D = \frac{\sqrt{2J\Omega}}{\hbar}\ . \tag{3.26}$$

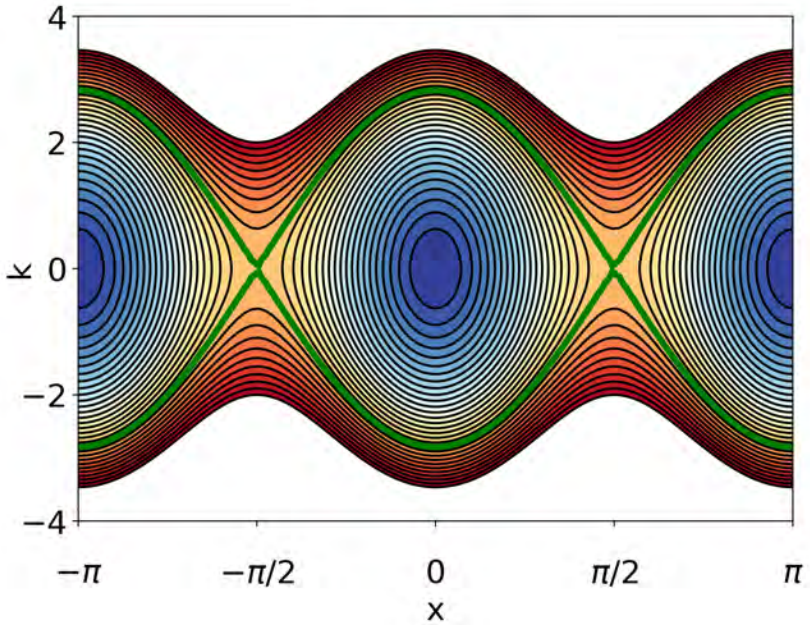

Figure 3.4: Classical phase space of the quasimomentum Hamiltonian 3.20. The thick green contours marks the separatix trajectories, as the boundary at which the dynamics changes.

Thus the solution of $k(t)$ and $x(t)$ is given as

$$k(t) = k\sin(\eta t)\ , \tag{3.27}$$

$$x(t) = -\frac{\hbar k}{2F_1}\eta\cos(\eta t)\ . \tag{3.28}$$

Hence in the phase space, $(x, p = \hbar k)$, the particle with a constant initial quasimomentum $k = k_o$, effectively follows rotational dynamics with frequency η having maximum displacement $x = \pm\frac{\hbar k d}{2\Omega}\eta$, around origin. The phase space generated is shown in Fig. 3.4 which elicits liberation over circular dynamics. The region of closed contours below the separatix is the threshold of simple dipolar motion near the origin of parabolic optical lattice. These are called dipole oscillations. While the liberation allude towards periodic switching of quasimomentum vector which quantum mechanically results in Bloch oscillations.

3.4.1 Mean Atomic Momentum

The above quasimomentum Hamiltonian maps on to a quantum pendulum model [Ponomarev and Kolovsky 2005] which effectively fences the possible dynamics in accord with the corresponding shifted trap origin. Eq. 3.27 encased with a width dependant function portraying the role of dephasing introduced by nonlinear spectrum of parabolic optical lattices, leads to the mean atomic momentum

$$\langle p(t) \rangle = p_o \, e^{-t^2/\tau_\sigma^2} \sin(\omega_B t), \tag{3.29}$$

where $\omega_B = \Omega l_o/\hbar$ is the Bloch frequency arising from coupled Eqs. 3.21 and 3.22 by standard separation of variable technique under a constant displacement to parabolic trap by l_o. The dynamics generated with above equation are shown in Fig. 3.5, which exhibit periodic modulation of oscillatory modes due to dephasing and revivals [Ayub and Saif 2012; Mahmud et al 2014; Saif 2000].

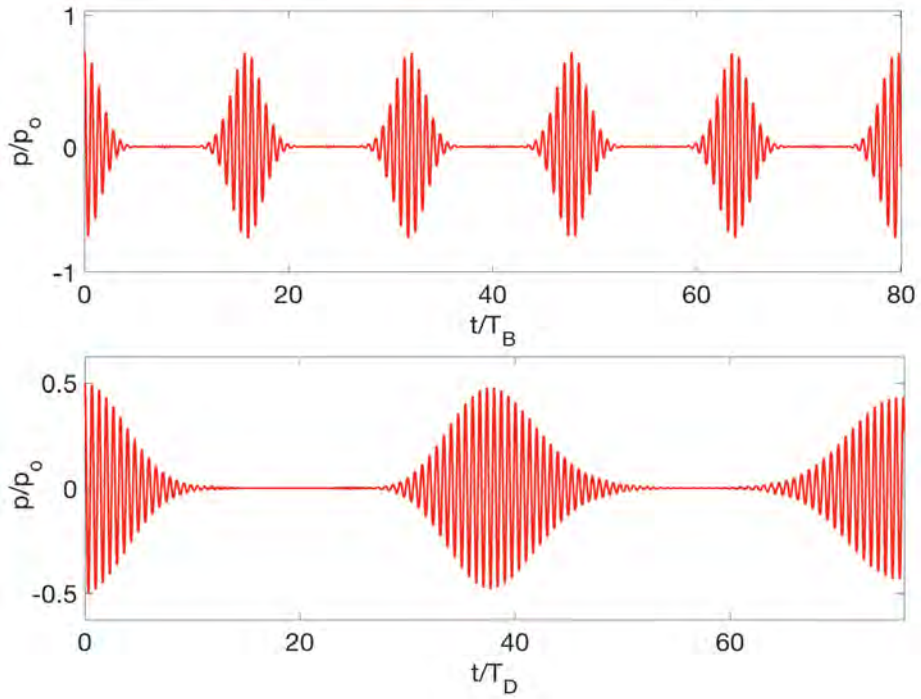

Figure 3.5: Single band dynamics of parabolic optical lattice. Bloch oscillations of the pendulum ground state at $l_o = 20$ (above) and Dipole oscillations for $l_o = 3$ (below) are shown with the separatix $l^* = 10$. Collapse and revival phenomenon is eminent caused by dephasing.

Having gathered all the initial information about the dynamical features induced by external potentials. We proceed towards actual single particle evolutions beyond the single band approximations. A thorough understanding of the parabolic optical lattice is developed in the next chapter where the dynamics are restricted to tight binding limits.

Chapter 4

Single Band Tight Binding Dynamics

An ultracold atom constrained to 'hop' between contiguous sites of an optical lattice in the vicinity of a spherically symmetric parabolic potential is an epitome of harmonic oscillator moving on a lattice. An initial description [Brand and Kolovsky 2007] uses a quantum pendulum model to expound the dynamical features. Although the general behaviour of overall eigenstates which play crucial role in systems's evolution was not considered. The eigenstates of the tight binding parabolic optical lattice are found to be given by special Mathieu functions [Rey et al 2005]. However, proceeding from the not so well known quasimomentum representation significantly clarifies many hidden aspects, unveiling modified dispersion relations and time evolution operators. Moreover, the dynamics generated with these evolutions considerably simplifies on working inside a fixed single band. Such an approximation along with the usual tight binding axioms is called single band tight binding model.

Bloch oscillation is the most celebrated quantum phenomenon, ever since surmised by Bloch [Bloch 1928] and extended by Zener [Zener 1934], in which a localised wave packet performs coherent oscillations under a constant linear forcing, due to band structure. Numerous applications of this have already been proven fertile. The question of Bloch oscillations under a quadratic forcing of parabolic potential is quite instinctive. Meanwhile, the concept of dipole oscillations has already been attached to parabolic optical potentials. In this chapter, the main character of energy eigenstates is discussed, which classifies both these dynamics.

4.1 Tight-Binding Features

Let us start with a single cold atom bound to move in a one dimensional periodic tight-binding lattice, described by Hamilton operator 2.29 in terms of Wannier states $|n,l\rangle$, with one localized orbital per site 'n'. The usual description of tight binding allows the atom to hop between nearest neighboring sites, while the motion is constrained to a finite region by an external parabolic confining trap. The Hamiltonian is

$$\hat{H} = -\frac{J}{2}\sum_n (|n\rangle\langle n+1| + |n+1\rangle\langle n|) + \frac{1}{2}\kappa d^2 \sum_n n^2 \ |n\rangle\langle n| \ , \tag{4.1}$$

where k represents the trap strength, d the lattice spacing, and J is the hopping matrix element, which is small compared to first band excitation energy. Also to simplify the notation, writing Wannier states, we have suppressed the band index l .

4.1.1 Modified Dispersion Relation

Alternatively, one can assign a description in terms of Bloch wave basis

$$|k\rangle = \sum_n |n\rangle\langle n|k\rangle = \sqrt{\frac{d}{2\pi}} \sum_n |n\rangle e^{inkd}, \tag{4.2}$$

which follows the identity $\langle n+1|k\rangle = e^{ikd}\langle n|k\rangle$, having quasi-momentum k limited to the first Brilloin zone $|k| \leq b$, with $b = 2\pi/d$. Using the relations

$$\sum_n \langle k'|n+1\rangle\langle n|k\rangle = e^{-ik'd}\frac{d}{2\pi}\sum_n e^{in(k-k')d} = \delta(k'-k)e^{-ikd}, \tag{4.3}$$

$$\sum_n n\langle k'|n+1\rangle\langle n|k\rangle = \frac{d}{2\pi}\sum_n n e^{in(k-k')d} = \delta(k'-k)\frac{x}{d} \tag{4.4}$$

we find that the lattice Hamiltonian 4.1 reduces to $\langle k'|H|k\rangle = d\delta(k'-k)H(k)$, with modified dispersion relation $H(k)$ written as:

$$H(k) = -J\cos(kd) + F_1 x^2 \ . \tag{4.5}$$

Clearly the above quasi-momentum Hamiltonian is diagonal, where the operators $e^{\pm ikd}$ implicit in the kinetic-energy term produces discrete lattice translations of the tunnelling atom and leads to the dispersion relation, for the case when there is no

external trapping potential,

$$E(k) = -J\cos(kd)\ . \tag{4.6}$$

Moreover, we have introduced the notation $F_1(=m\omega_\tau^2/2)$ for the half of the trap strength to highlight the notion of force on atom, whenever it moves away from the trap origin [Saif and Watanabe 2019]. This force provided by the parabolic trap is inhomogeneous, which increases quadratically from each side of the center of trap. To include the effects induced by quardatic forcing, the trap origin is shifted by distance $s = \Delta x$ to new equilibrium position $l_o = \Delta x/d$, this will also set the particle into motion.

4.1.2 Energy Spectrum

To include the initial displacement of trap we begin with

$$H(k) = -J\cos(kd) + F_1 s^2\ , \tag{4.7}$$

here $s = x - x_o$. As we take the canonically conjugate variables $u = kd/2$, $s = i\frac{\partial}{\partial u}$ and solve the discrete nonlinear Schrodinger equation (DNLS), we end to a Mathieu equation

$$\left[\frac{\partial^2}{\partial u^2} + \left(\frac{4E}{\Omega}\right) - 2\left(\frac{-2J}{\Omega}\right)\cos(2u)\right]\psi(u) = 0\ , \tag{4.8}$$

with corresponding Mathieu characteristic value $4E/\Omega = \alpha$ and kinetic energy parameter $-2J/\Omega = q$, which mainly scales with the parabolicity $\Omega = F_1 d^2$. The eigenstates of the system are typically known periodic Mathieu Functions. Using Floquet solution [Abramowitz and Stegun 1964] we write

$$\psi_r(s,\nu) = \sqrt{\frac{d}{2\pi}}\, C_m^r(\nu) \sum_m e^{[i(\nu+2m)K]}\ , \tag{4.9}$$

to the appropriate normalisation over first Brillouin zone. Whereas the coefficients $C_m^r(\nu)$ mainly depend upon ν, the characteristic Floquet exponent, and are given by difference equation

$$[\alpha_r(q,\nu) - (\nu+2m)^2]C_m^r(\nu) = q[C_{m-1}^r(\nu) + C_{m+1}^r(\nu)]\ . \tag{4.10}$$

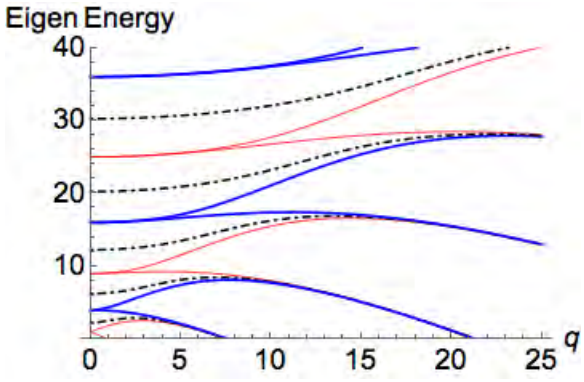

Figure 4.1: Schematic illustration of the Mathieu characteristic energies as a function of parameter q. Solid dark blue (light red) curves are the eigen values related to a_r (b_r), whereas dotted-dashed lines correspond to λ_r, with $\nu = 0.5$.

In above relation, $\alpha_r(q, \nu)$ represents the corresponding rescaled energy eigenvalues and the energy of a state with quantum number 'r' reads

$$E_r = \begin{cases} \frac{\Omega}{4} a_r(q) & ; \quad even \\ \frac{\Omega}{4} b_{r+1}(q) & ; \quad odd \,, \end{cases}$$

where $a_r(q)$ and $b_{r+1}(q)$ describe the characteristic energies of α [Abramowitz and Stegun 1964; Meixner and Schäfke 1954]. Note that the energy spectrum varies depending upon the choice of ν, which commensurate with the order of Mathieu equation by relation $r = \nu \pm 2z$. Hence the quantum number r is rounded of to the nearest even integer $2z$. Now for integer values $r = \nu$, which is the case in above mentioned solution. It is worth mentioning that there also exists a second solution to the above equation, which is well known by the name of Mathieu functions for non-integer order. In that scenario the eigenstates are specified by $me_\nu(u, q)$, with corresponding characteristic eigen energies $\lambda_{\nu+2z}(q)$, uniquely describing both even and odd solutions.

The first few levels that appear from both these cases are, shown in Fig. 4.1, plotted across the parameter q. Where the continuous solid lines represent energy spectrum for integer order, irrespective of the even and odd Mathieu functions living in quasi-momentum space. Both of these solutions have definite parity, with odd levels (dark blue) of these characteristics are 2π periodic and the even levels (light red) are π periodic. In particular, Mathieu functions for non-integer order are also plotted to

distinguish the energy spectra. They are shown as dotted-dashed lines in Fig. 4.1, in which each quantum number takes on an additional fractional constant number, i.e. $\nu = 0.5$. By this the spectrum modifies itself and the eigenvalues mainly lie over a single curve, which for our taken parameters falls exactly in between the first solution bands.

Some more insight can be drawn by looking at the Fig. 4.1 which also highlights a couple of other bounding features. One of which is the case of $q \to 0$, where the spectrum approaches to the quardaticaly-spaced free particle energy levels. This behaviour is clearly eminent from the figure as well as from Eq. 4.8, which completely reduces to the free particle Schrodinger equation whenever q vanishes. To further elaborate the trends in this region we have the following asymptotic expression, for small q [Rey et al 2005],

$$E_r = \frac{\Omega}{4}\left\{r^2 + \frac{1}{2(r^2-1)}q^2 + \frac{5r^2+7}{32(r^2-1)^3(r^2-4)}q^4 + \dots\right\}. \tag{4.12}$$

Another important point upon which we would like to emphasise on is the origin of localized eigenstates in this regime. Wavefunctions approaching free particle solution in momentum space will bring maximally localized eigenstates in the position space, and the particle will sit on a single lattice site, with maximum probability amplitude on it. Localization of the wavepacket is a prerequisite for some key dynamical phenomena like Bloch oscillation which we construe in detail in next subsections.

Second bounding case appears in the $q \to \infty$ limit of this problem, which is singular in the sense that the spectrum is entirely different from that of the translationally invariant lattice ($\Omega = 0$). In this regime, for very large values of kinetic energy parameter q, we have the asymptotic expansions

$$E_r = \frac{\Omega}{4}\left\{-2q + 4\sqrt{q}\left(r+\frac{1}{2}\right) - \frac{(2r+1)^2+1}{8} + \frac{[(2r+1)^3+3(2r+1)]}{128\sqrt{q}} + \dots\right\}. \tag{4.13}$$

Ignoring higher order terms and restricting ourselves to the quantum numbers linear

in l, above expression approximates to

$$E_r = -J + \sqrt{2J\Omega}\left(r + \frac{1}{2}\right) , \tag{4.14}$$

these are the famous equi-spaced harmonic oscillator eigenenergies, displaced by amount $-J$ from the bottom. Thus the Hermite eigenfunctions corresponding to these energies will also be shifted and haing the new origin at point l_o. The atom will perform simple dipolar motion with an effective dipole frequency, $\omega_D = \sqrt{2\Omega J}/\hbar$. These transitions are also evident by looking at the Fig. 4.1, where one can see the energy curves merging over a single line, which becomes equally spaced as well at the right extreme. This is a unique behaviour, because in the absence of the harmonic trap the eigen functions in postion space are Bloch states, but here for a diminishing trap strength one encounters something different. This effect is thoroughly explained in [Hooley and Quintanilla 2004], where the authors reveal another counter characteristic of the system, in this regime, i.e. the eigenstates becomes more and more localized by increasing r. Now lets examine the dynamical modes of the system as the energy eigenstates interlace between localized to extended states.

4.1.3 Eigenstates

Before describing the time propagation, let us analyse the eigensfunctions in real space,

$$\begin{aligned}\psi_r(s,\nu) = \langle s|\psi_r\rangle = \sqrt{\frac{d}{2\pi}}\int_{-\frac{\pi}{d}}^{\frac{\pi}{d}} dk \langle s|k\rangle\langle k|\psi_r\rangle = \frac{d}{2\pi}\sum_m C_m^r(\nu)\int_{-\frac{\pi}{d}}^{\frac{\pi}{d}} dk\, e^{iks}.e^{\frac{i}{2}(\nu+2m)kd} \\ = \frac{d}{2\pi}\sum_m C_m^r(\nu)\int_{-\frac{\pi}{d}}^{\frac{\pi}{d}} dk\, e^{i[(x-l_o+\frac{\nu d}{2}+md)k]} = \sum_m C_m^r(\nu)\,\delta(x-l_o+\nu d/2+md).\end{aligned} \tag{4.15}$$

This represents a collection of delta functions defining the discrete Hilbert subspace $x = nd$, and the diminishing argument of the Dirac delta function, in above expression, deduce that the characteristic Floquet exponent proportionate with the initial displacement l_o, by relation $\nu = 2l_o/d$. Now the eigenstates becomes a function of the initial displacement of the trap and the coefficients $C_m^r(\nu)$ describe the real space amplitude, which sweeps across the whole lattice, as m varies. Therefore, ν being integer or non-integer decides the points where maximum amplitudes reside. This for

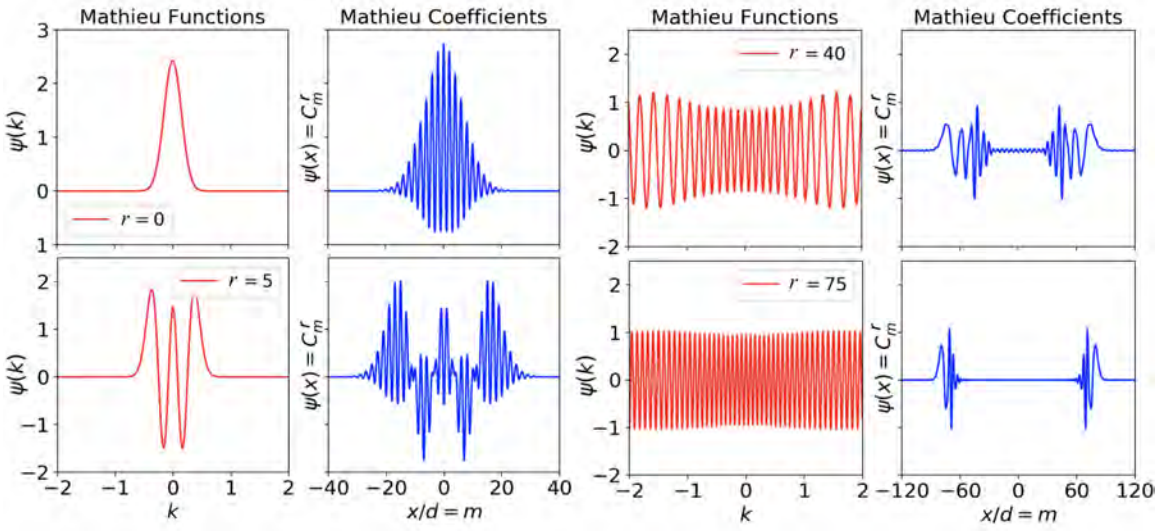

Figure 4.2: Eigen functions for r = 0, 5, 40, 75 are shown in quasimomentum representation, starting from left, each with their corresponding spatial analog placed right together it, for constant values of $q = -500$ and $\nu = 0.5$, as obtained by solving Eq. 4.10.

integers lie exactly above or half way between each lattice site, corresponding to the 2π or π periodic solutions, respectively, when odd or even values of ν are considered. For ν non-integer, the non-trivial solution discussed above, is dropped with the understanding that the real space eigenstates vanishes uniformly over each lattice site. Hence only π and 2π periodic Mathieu functions are considered as valid solutions in k-space, which give rise to even and odd amplitudes $C_m^r(\nu)$ in position space. Generally, we can say that the presence of external trapping takes the Bloch states to the k-space, with the equivalent delta functions envelope generating maximally localized Wannier states in real space.

The overall behaviour of eigenstates as obtained via exact diagonalization of Eq. 3.10, is shown in Fig. 4.2, both in the quasimomentum and spatial description. All these plots associate with fixed parametric values, that are $q = -500$ and $\nu = 0.5$, which depict similar behaviour to discretized harmonic oscillator for lower lying states, but is still not the same. Although it can be shown that for large values of $|q|$ the eigenstates took the exact shape of Hermite polynomials, as known analytically. The wiggles appearing in the spatial profiles related to first two quasimomentum eigen-

states are responsible for the fact that there will be many such periodic functions of the same form in k-space and they sums up to a single localized packet as connected by the fourier transform. The localization effect of high energy states away from the center of parabolic potential is also visible by looking at the right extreme of Fig. 4.2. Remember that here we have chosen a moderate value of kinetic energy parameter q, which can be controlled in experiment and for very smaller values we can see localization effect emerging right from the ground state (not shown).

4.2 Bloch Osillations

The time evolution operator $\hat{U}(t)$ in Bloch wave basis is simply

$$\begin{aligned} \hat{U}_{k',k}(t) = \langle k'|\hat{U}(t)|k\rangle &= \sum_r \langle k'|\psi_r\rangle e^{-iE_r t/\hbar}\langle\psi_r|k\rangle \\ &= \frac{d}{2\pi}\sum_{r,m} C_m^r(\nu)C_m^{r*}(\nu)e^{-i(k-k')\nu}e^{-2im(k-k')}e^{-iE_r t/\hbar}\,, \end{aligned} \tag{4.16}$$

this propagator changes based on the inherent eigenenergies, which were earlier segregated into two prominent regimes. Keeping in mind that for the solutions that sustains in our problem $r = \nu$, meanwhile ν itself connects with l_o. Using Eq. 4.12 we write

$$\begin{aligned} \hat{U}_{k',k}(t) &= \frac{d}{2\pi}\sum_{r,m} C_m^r(\nu)C_m^{r*}(\nu)e^{-2im(k-k')}e^{-i(k-k')\nu}e^{-i\Omega r^2 t/4\hbar}\dots \\ &= \sum_m C_m^r(\nu)C_m^{r*}(\nu)e^{-2im(k-k')}\delta(k-k'+\Omega l_o t/\hbar d)\dots\,, \end{aligned} \tag{4.17}$$

which defines a local static force $F = \Omega l_o/d$, and we see that the quasi-momentum k' follows the classical acceleration

$$k' = k_t = k - Ft/\hbar\,. \tag{4.18}$$

And the usual lattice band picture restricts the quasimomentum k to first Brillouin zone. Hence in low q regime the atom will perform Bloch oscillations with frequency $\omega_B = \Omega l_o/\hbar$, remaining constrained to one side of the trap.

In the basis of Wannier states, propagator takes the form

$$\begin{aligned}\hat{U}_{n,m}(t) = \langle n|\hat{U}(t)|m\rangle &= \sum_r \langle n|\psi_l\rangle e^{-iE_r t/\hbar}\langle \psi_r|m\rangle \\ &= \sum_r C_n^r(\nu) C_m^{r*}(\nu) e^{-iE_r t/\hbar} \ ,\end{aligned} \tag{4.19}$$

the Fourier counterpart of 4.16. Here $C's$ are the spatial amplitudes already described in the previous section. The time evolution operator can be simplified by substituting asymptotic expressions 4.12 and 4.13, which divides the system's evolution into two dynamical modes, namely Bloch mode and Dipole mode. Further, one can see that evolution operator is periodic in both regimes with Bloch period $T_B = 2\pi\hbar/\Omega l_o$ and Dipole period $T_D = \sqrt{2}\pi\hbar/\sqrt{\Omega J}$. Lets examine wave packet evolution in both scenarios one after the other.

Consider the complete time evolution operator, with discrete basis, acting upon an initial state ψ_o as

$$\begin{aligned}|\psi(t)\rangle = \left(\sum_{n,m} \hat{U}_{n,m}(t)|n\rangle\langle m|\right)|\psi(0)\rangle &= \sum_{n,m,l} C_n^r(\nu) C_m^{r*}(\nu) e^{-iE_r t/\hbar}|n\rangle\langle m|\psi(0)\rangle \\ = \sum_{n,m,r} C_n^r(\nu) C_m^{r*}(\nu) e^{-iE_r t/\hbar} C_m(0)|n\rangle &= \sum_n C_n(t)|n\rangle \ ,\end{aligned} \tag{4.20}$$

where, $C_m(0)$ counts for the spatial distribution of initial wave packet, over the finite lattice Hilbert subspace. Whose time evolution is governed by $C_n(t)$, connate with the ingrained quasi-energies.

Bloch oscillations of a preliminary state ψ_o is shown in Fig. 4.1, which depict a couple of illustrating instances, in the low q regime, used to expound the dynamical sensitivity of the system, towards the initially projected wave function. That is, if the overall amplitude of the initial state particularly reside in a single quantum well, then the wave packet will perform coherent Bloch breathing, uniformly spreading towards both spatial extremes, after which a complete reconstruction is observed on the same outset at each Bloch period. Other than that is the case of an extended primary distribution populating more than one nearby lattice sites. Such a broad Gaussian distribution is taken as the initial state in right of Fig. 4.1, having non-zero

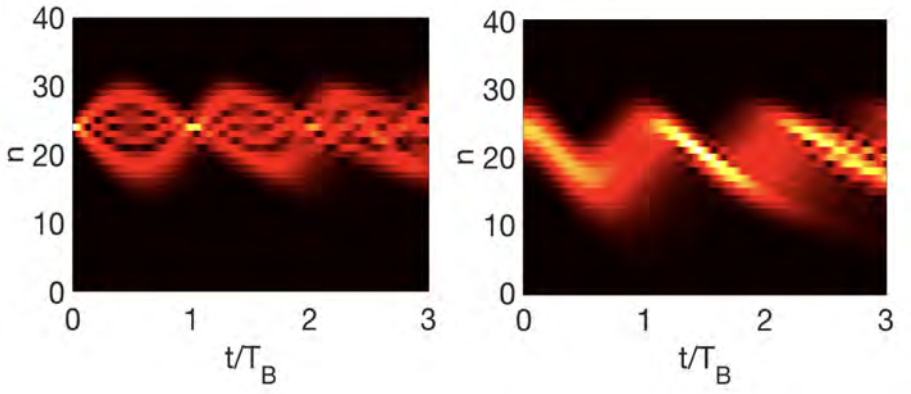

Figure 4.3: Time evolution of the absolute value of the wavefunction $|\langle n|\psi(t)\rangle|$ as a function of t/T_B and n, exhibiting Bloch Breathing mode of a localized wavepacket initially placed at $l_o = 24$ (left), and center of mass Bloch oscillations for a broad Gaussian wavepacket with variance $\sigma = 1.5$ and mean $a = 24$ (right), in the tight binding model at $|q| = 162.5$.

probability amplitude over several contiguous wells. The inceptive distribution now undergoes dispersionless center of mass Bloch oscillations. Both these plots are generated at a fixed value of $|q| = 162.5$ (Hamburg experiment [Heinze et al 2013]) and a trap shift to $n = 24$. One can easily note the wavepacket hampering on one side of the parabolic optical lattice, although there is no physical boundary.

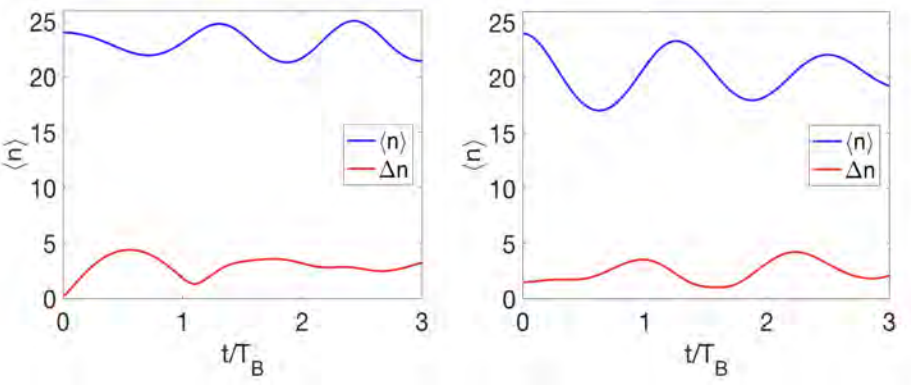

Figure 4.4: Expectation values and width of scaled position, for the same wave packets as used above, at zero initial momentum.

4.3 Dipole Oscillations

Dipole oscillations of atomic wave packets have been largely studied in parabolic optical lattices, which gather more attention right after the realisation of BECs. A lot of work has been done in this regard, both theoretically [Pezzè et al 2004; Polkovnikov et al 2002; Rey et al 2005; Ruuska and Törmä 2004] and experimentally [Cataliotti et al 2003; Fertig et al 2005]. This harmonic oscillator character is pretty evident from the underneath energy spectrum, in the high q regime. And the Hermite eigenfunction are simply displaced from the bottom, by amount J, with centre on the new equilibrium position l_o. With Eq. 4.14, the real space propagator takes the form

$$\hat{U}_{n,m}(t) = \sum_r C_n^r(\nu) C_m^{r*}(\nu) e^{-\left[i\frac{\sqrt{2J\Omega}}{\hbar}\left(r+\frac{1}{2}\right)-J\right]t} . \tag{4.21}$$

Thus the wavepacket transverses both sides of parabolic optical lattice, in the high q regime, performing center of mass dipolar motion with an effective frequency $\omega_D = \sqrt{2\Omega J}/\hbar$. The dynamics generated are shown in Fig. 4.5. The time axis is scaled with the corresponding dipole period.

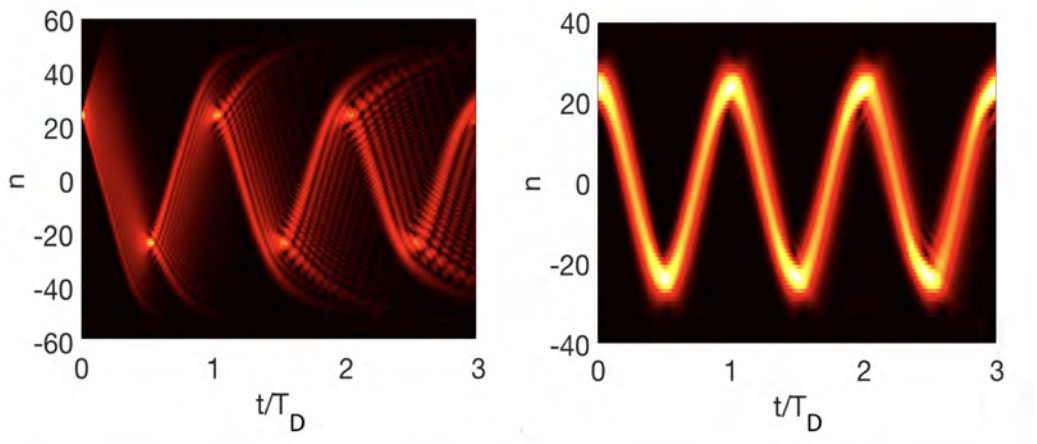

Figure 4.5: Time evolution of the absolute value of the wavefunction $|\langle n|\psi(t)\rangle|$ as a function of t/T_D and n, exhibiting dispersive dipole oscillations for a sharply localized wavepacket at $l_o = 24$ (left), and simple dipolar motion for a broad Gaussian wavepacket with variance $\sigma = 1.5$ and mean $a = 24$ (right), in the tight binding model with $|q| = 1625$.

In our numerical simulation the high q regime is achieved by reducing the trap strength Ω ($= 2.79 \times 10^{-4} E_r$, previously) by order of tens. Although it can also be done by enhancing the lattice tunnelling J ($= 2.27 \times 10^{-2} E_r$; see appendix for the relevant energy scale) through depth V_o. As parabolic trap is an external component so it is preferred for the sake of simplicity. Prominent changes in the dynamics is observed at $|q| = 1625$, which approaches to coherent dipole oscillations for a broad initial distribution, as shown in Fig. 4.5. While a sharply localized distribution suffers significantly expanding through the contiguous wells, although the overall transport is still very much similar.

To further construe such effects, an elementary method is mostly used while studying Bloch oscillations. That is by calculating the expectation values one could easily discern the established wavepacket dynamics. Moreover, the Ehrenfest theorem ingrained to expectation values also serves as a good test to the computations. Therefore expectation values and position variances are calculated for both modes, as shown in Fig. 4.4 and Fig. 4.6. Small changes in variances are observed for Bloch oscillations. Despite, for Dipole oscillations fluctuating variances are seen which becomes more robust as the time goes on. The average atomic motion is also pretty much eminent.

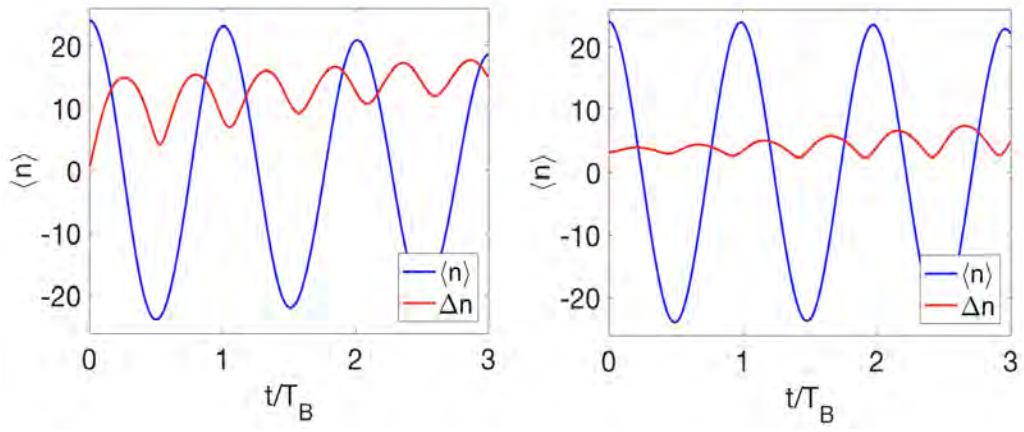

Figure 4.6: Expectation values and width of scaled position, for the same wave packets used in dipole oscillations at a zero initial velocity. Dephased oscillations are observed with fluctuating variances.

Note : Although it was expected that the quadratic forcing of parabolic trap should modify the Bloch oscillations.A complete breakdown of coherent oscillations is observed [Geiger et al 2018], confirming the single band approximation results of previous chapter. Also, the dipole oscillations are found to be dephased after few cycles.

Chapter 5

Wave Packet Propagation

The actual wave packet evolutions beyond all approximations are at the heart of this chapter. Having understood the lack of comprehensiveness in analytical solutions for the parabolic optical lattice Hamiltonian, we proceed towards present day computational advancements to check the reliability of the estimated results. Spectral split operator technique is being employed, for the wave packet propagations, which is an accurate method, widely used for calculating exact time dependences. This allows us to probe beyond tight binding or single-band approximation. Such numerical evaluations are now common and we adduce to [Hartmann et al 2004] for similar studies.

5.1 Beyond Single Band Approximation

The Landau zener tunnelling phenomenon merely the consequence of inter-band coupling was completely ignored in previous chapters, being restricted to a fixed single band. The Schrodinger equation of parabolic optical lattice Hamiltonian 2.22 was completely non-integrable in real space. For that reason we turned to quasimomentum representation and solved the tight binding version of the system. However, the exact general form of eigenstates and energy spectrum is still abstruse. Such a scenario mostly builds up in the course of driven systems, where the Hamiltonian takes on explicit time dependent terms. Most often analytical solutions become sparse and computational methods are employed. We proceed likewise and solve the problem numerically for better definite results.

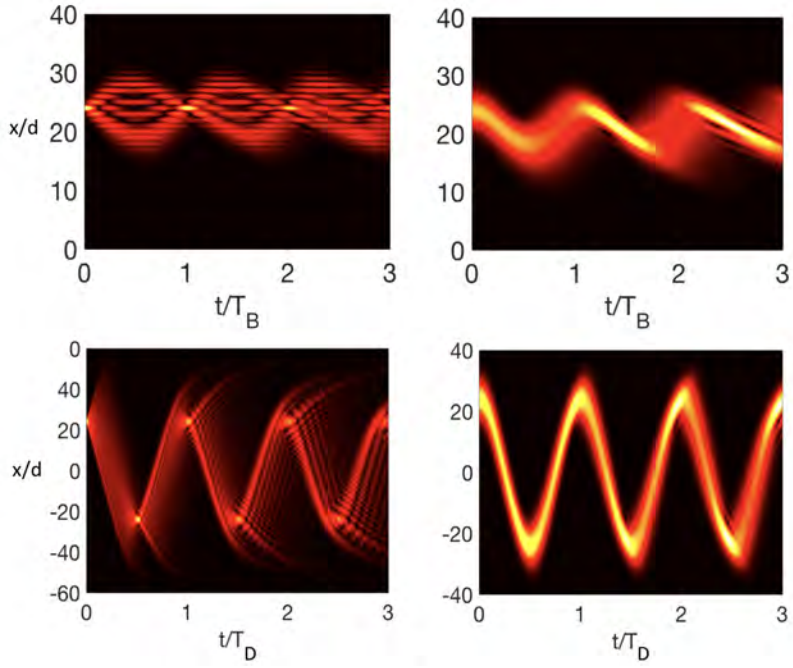

Figure 5.1: Propagation of a Gaussian wavepacket with width as previously taken to be in tight binding evolutions. Absolute value of the wavefunction is shown, exhibiting Bloch (top) and Dipole (bottom) oscillations, where $s = 10E_r$ and $\nu = 2.83 \times 10^{-5} E_r$. The latter is reduced by one order of magnitude for the Dipole oscillations.

The dynamics of a single atom in effect of the Hamiltonian 2.22 are governed by the time dependent Schrödinger equation

$$i\hbar_{eff}\frac{\partial\psi}{\partial t} = -\frac{\partial^2\psi}{\partial y^2} + (s\sin^2(y) + \nu y^2)\psi, \tag{5.1}$$

where y, $\hbar_{eff}$ and ν denote the rescaled position $y = k_L x$, the rescaled Planck's constant $\hbar_{eff} = \Omega l_o/\pi$ and the scaled parabolicity $\nu = \Omega/\pi^2$, respectively, with $s = V_o/E_r$. The whole scaling assembly is given in the Appendix, where we also highlight the scaled parametric values used. We stick to the values of Hamburg experiment [Heinze et al 2013]. The experiment is preferred for the ease of controllable lattice depth s and tuneable parabolicity ν, although Aarhus experiment [Pedersen et al 2013] serves equally well in wave packet production and manipulation. The new parameters introduced and the scaled values are given in the Table 7.1.

Above equation can fairly be solved by means of an operator splitting method [Feit

et al 1982]. The technique splits the evolution operator $e^{-i[T(k)+V(x)]t/\hbar}$ into corresponding kinetic and potential parts, using Baker-Hausdorff formula, which are separately calculated in there respective space. Considering only the lower order terms of expansion, the evolution is governed by

$$e^{-\frac{i}{\hbar}Ht} = e^{-\frac{i}{\hbar}\frac{V(x)}{2}t} e^{-\frac{i}{\hbar}T(k)t} e^{-\frac{i}{\hbar}\frac{V(x)}{2}t} \ . \tag{5.2}$$

Fourier transform of the operators $e^{-iT(k)t/\hbar}$, $e^{-iV(x)t/\hbar}$ transforms the initial state in configuration space (from one to the other). However, the space you wanna end to is first projected on to the initial state. Keeping the same value of parabolicity as previously chosen to be in tight binding approach, $\nu = 2.83 \times 10^{-5} E_r$, parameters of the physical system reduces to only one variable, i.e. scaled depth of the optical potential s. For $s \geq 4$ the system strictly follows tight binding dynamics. With $s = 10E_r$ and at the same initial conditions, the results obtained here, Fig. 5.1, practically coincide with the tight binding evolutions of previous chapter.

Further, the depth of optical potential is reduced to see beyond the tight binding approximation. The scaled values are $s = 3.6E_r$ and $\nu = 2.83 \times 10^{-5}$. As an initial state, we use the displaced ground state of the system and, hence, width of the wave packet is no more an independent parameter. The ground state of the Hamiltonian 2.22, with center of the harmonic potential shifted to Δx, is found by imaginary time propagation of some trial wavefunction. For the real time propagations then, Eq. 5.1 is solved. This has the same effect as suddenly displacing the ground state wave function. In the Catiliotti experiment [Cataliotti et al 2003], this has been achieved by means of a weakly interacting (dilute) Bose-Einstein condensate, where the atomic cloud is shifted by displacement of the magnetic trap. It could also be obtained by initial driving as engineered in [Sherson et al 2012]. Therefore, we posit that Hamburg experiment [Heinze et al 2013] may serve equally well, where the parametric values are more favourable for observing the discussed dynamical phenomena.

Fig. 5.2 shows the Bloch mode, in real space, as a function of time (shown is the probability density $|\psi(x,t)|^2$ over initial four Bloch periods, where the bright regions corresponds to higher density). At $t = 0$, the wavepacket segregates instantly and the subsequent dynamics results in the superposition of Bloch and Dipole oscillations.

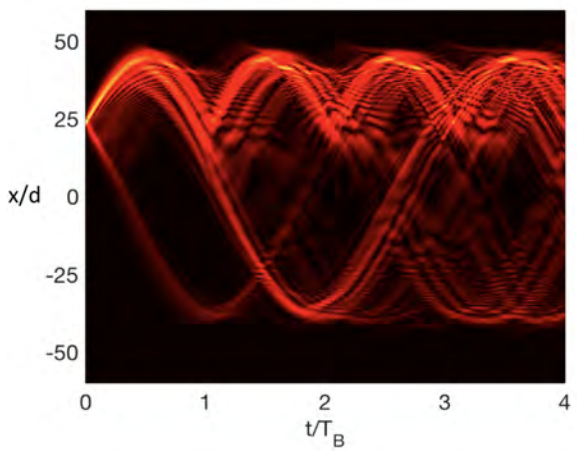

Figure 5.2: Propagation of the displaced ground state of the system. Absolute value of the wavefunction is plotted as a function of t/T_B and x/d, exhibiting Landau-Zener tunnelling over Bloch oscillations, where $s = 3.6E_r$ and $\nu = 2.83 \times 10^{-5}E_r$.

The splitting is repeated with a decreasing amplitude at each Bloch period. This behaviour can be explained on the basis of band structure involved. Band structure reflects the periodicity of the lattice and it is well known that band gap reduces at lower depths of the optical potentials. Therefore, at lower band gaps the interband coupling could no more be neglected. Hence, as we probe beyond tight binding approximation, interband coupling gives rise to Landau-Zener transitions [Yamakoshi and Watanabe 2015]. Thus numerically observed splitting is due to perceptible contributions from higher bands.

5.2 Oscillation Vs. Acceleration

Till now the research literature ascribes the motion of Landau Zener tunnelling fraction to uniform acceleration, as the course of homogeneously tilted lattices [Hartmann et al 2004]. However, here we report the dipole oscillations of the accelerated part of the wavepacket, due to symmetry of the parabolic optical lattice. It can easily be seen from Fig. 5.2 that while performing Bloch oscillations, on one arm of the symmetric structure, some fraction of the wavepacket segregates itself from the overall multitude and starts to oscillate in the higher bands, traversing both sides of parabola. Hence, in parabolic optical lattices there will be complete oscillations [Ali et al 2019] and a properly trapped atom can never escape from the lattice during its propagation.

Chapter 6

Conclusion

With all this understanding developed, we are in a comfortable position to segregate the dynamical phases of the parabolic optical lattice. A phenomenological illustration is shown in Fig. 6.1, where we have marked the fences of Bloch and Dipole oscillations, using the relation

$$n_c = 2\left|\sqrt{\frac{q}{2}}\right| \ , \tag{6.1}$$

being the critical eigen number at which the behaviour of eigenstates changes for a general value of q. Above the critical number the eigenstates are localised, while they are extended, in space, below it [Rey et al 2005]. Consequently, it is inferred that near the centre Dipole oscillations will be observed and on the uprise sides of parabola Bloch oscillations dictate the dynamics. A clear boundary by blue dotted lines is marked on the ground band, in Fig. 6.1. The regions 4 and 7(8) strictly corresponds to Dipole and Bloch oscillation, respectively.

The unique effect of oscillating Landau-Zener tunnelling thoroughly described in previous chapter is also shown along with, where the first excited band is shown by red parallel lines. It can be seen that the regions $1, 2, 3$, marked with a blue pointer, clearly, depict the band energy overlap. Although Landau-Zener tunnelling is a purely quantum phenomenon, which could also occur in 4 and 7(8) at smaller band gaps, we only mark here the persistent domain of moderate tunnelling probabilities.

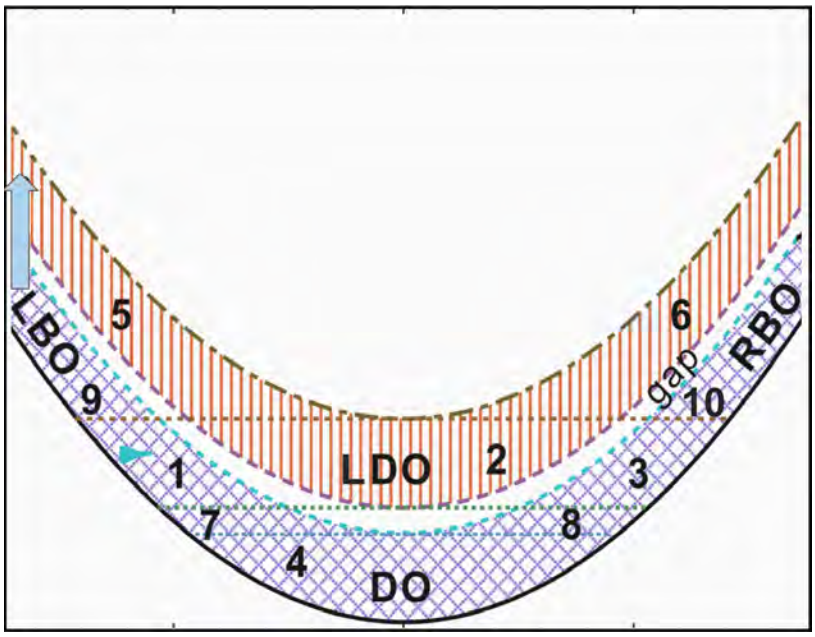

Figure 6.1: Phase diagram of parabolic optical lattice. Regions of Bloch and dipole oscillations are marked on the ground band (bottom), whereas the Landau-Dipole oscillations disseminate across the whole lattice in the first band (top).

The oscillations of Landau-zener tunnelled fraction can also be understood from the presented symmetric structure. Wave packet accelerates from one uprise arm (5 or 6), hindering the Left and Right Bloch oscillations (LBO-RBO), crossing the centre it again traps into a potential hill. Consequently, it de-accelerates giving rise to oscillations, called Landau-Dipole oscillations (LDO).

It is to be noted that all the dynamical phases relates with fixed energy domains, which can be attained by placing the wave packet at corresponding displaced positions. One easy way used is shifting the eigenstates by a sudden shift l_o to the parabolic trap centre. For a localized wave packet created near the edges of parabola, with high values of trap shift, the rate of Landau-Zener tunnelling is much higher (see pointer) and Landau-Dipole oscillations pertains with larger amplitudes.

Hence, it is inferred that parabolic optical lattice is the core of rich dynamical features. The results obtained are experimentally viable, which will be having potential applications in matter wave splitting and waveguiding devices [Ali and Saif 2019].

Appendix: Units

Rescaling and Parametric Values

In the following, we are giving a description of the used scaled units. The system of units is motivated by use of recoil energy, $E_r = \frac{\hbar^2 k_L^2}{2m}$, and reducing the number of free parameters to a minimum [Yamakoshi et al 2016]. The scaled hamiltonian yields dimensionless variables, which can easily be used in numerics. Starting with the parabolic optical lattice

$$H = \frac{p^2}{2m} + V_o \sin^2(k_L x) + F_1 x^2 \ . \tag{6.2}$$

The hamiltonian scaled with the free particle energies can be written as

$$H_{eff} = -\frac{\partial^2}{\partial y^2} + s \ \sin^2(y) + \nu y^2 \ , \tag{6.3}$$

where y, s, and ν denote the rescaled position $y = k_L x$, the rescaled optical lattice depth $s = V_o/E_r$, and the rescaled parabolic trap strength $\nu = m\omega_T^2/2E_r k_L^2$, respectively.

Experimental parameters(Aarhus)				Converted parameters		
λ	m (^{87}Rb)	ω_0	E_r	s	ν	J
914 nm	1.44×10^{-25} kg	$40.6 \times 2\pi$Hz	1.81×10^{-30} J	16 E_r	$5.51 \times 10^{-5} E_r$	$6.06 \times 10^{-3} E_r$
Experimental parameters(Hamburg)				Converted parameters		
λ	m (^{40}K)	ω_0	E_r	s	ν	J
1030 nm	6.64×10^{-26} kg	$50.0 \times 2\pi$Hz	3.12×10^{-30} J	10 E_r	$2.83 \times 10^{-5} E_r$	$2.27 \times 10^{-2} E_r$

Table 6.1: Typical values of the parameters for Aarhus and Hamburg experiment [Yamakoshi and Watanabe 2015]. Parameters converted for numerical analysis are also shown.

The scaled variables are shown in Table 7.1, with precise values calculated from the recent experiments. Both experiments report high fidelity generation of coherent matter wave packets in parabolic optical lattice. Although the experiments were strictly performed to transfer the matter wave packets to higher bands by lattice modulation. We restrict ourselves to the modulation free system for now, leaving the modulation effects a future endeavour.

Bibliography

Abramowitz I. and Stegun I. A. (1964). *Handbook of Mathematical Functions, National Bureau of Standards.*

Ali U., Medhat S., and Saif F. (2019). *Dynamics of ultracold atoms in parabolic optical lattice.* (submitted).

Ali U. and Saif F. (2019). *Recurrence dynamics in parabolic optical waveguide arrays.* (to be submitted).

Anderson M. H., Ensher J. R., Matthews M. R., Wieman C. E., and Cornell E. A. (1995). *Observation of Bose-Einstein condensation in a dilute atomic vapor below 200 nanokelvin.* Science, 269(198).

Ashkin A. (1970). *Acceleration of trapping of particles by radiation pressure.* Phys. Rev. Lett., 24(156).

Ayub M. (2012). *Cold atoms in driven optical lattices.* PhD thesis, Quaid-i-azam University.

Ayub M., Naseer K., Ali M., and Saif F. (2009). *Atom optics quantum pendulum.* Journal of Russian Laser Research, 30(3).

Ayub M. and Saif F. (2012). *Delicate and robust dynamical recurrences of matter waves in driven optical crystals.* Phys. Rev. A, 85(023634).

Battesti R., Cladé P., Guellati-Khélifa S., Schwob C., Grémaud B., Nez F., Julien L., and Biraben F. (2004). *Bloch oscillations of ultracold atoms: A tool for a metrological determination of h/m˙Rb.* Phys. Lett. A, 92(253001).

Biao W., Yong X., Lin D., and Jun-Ren S. (2012). *Self-consistent approach for mapping interacting systems in continuous space to lattice models.* IOP Science, 29(8).

Bloch F. (1928). *About the quatum mechanics of electrons in crystal lattices.* Z. Phys., 52(555).

Bloch F. (1929). *Uber die Quantenmechanik der Elektronen in Kristallgittern.* Z. Phys., 52(555).

Bloch I. (2005). *Ultracold quantum gases in optical lattices.* Nature Physics, 1(23).

Bloch I., Dalibard J., and Zwerger W. (2008). *Many-body physics with ultracold gases.* Rev. Mod. Phys., 80(885).

Bloom B. J., Nicholson T. L., Williams J. R., Campbell S. L., Bishof M., Zhang X., Zhang W., Bromley S. L., and Ye J. (2014). *An optical lattice clock with accuracy and stability at the 10ˆ-18 level.* Nature, 506(71).

Bouchard A. M. and Luban M. (1995). *Bloch oscillations and other dynamical phenomena of electrons in semiconductor superlattices.* Phys. Rev. B, 52(5105).

Bradley C. C., Sackett C. A., Tollett J. J., and Hulet R. G. (1995). *Evidence of Bose-Einstein condensation in an atomic gas with attractive interactions.* Phys. Rev. Lett., 75(1687).

Brand J. and Kolovsky A. R. (2007). *Emergence of superfluid transport in a dynamical system of ultra-cold atoms.* The European Physical Journal D, 41(2).

Cataliotti F. S., Fallani L., Ferlaino F., Fort C., Maddaloni P., and Inguscio M. (2003). *Superfluid current disruption in a chain of weakly coupled Bose–Einstein condensates.* New J. Phys., 5(71).

Chin C., Grimm R., Julienne P., and Tiesinga E. (2010). *Feshbach resonances in ultracold gases.* Rev. Mod. Phys., 83(1225).

Courteille P. W., Bagnato V. S., and Yukalov V. I. (2001). *Bose-Einstein condensation of trapped atomic gases.* Laser Phys., 11(659).

Dalibard J. and Cohen-Tannoudji C. (1985). *Dressed-atom approach to atomic motion in laser light: the dipole force revisited.* Journal of the Optical Society of America B, 2(11).

Davis M. J. and Blakie P. B. (2006). *Critical temperature of a trapped Bose gas: comparison of theory and experiment.* Phys. Rev. Lett., 96(060404).

Dubius N. (2009). *Superfluid to Mott-insulator transition of cold atoms in optical lattices.* Phys. B: Condense Matter, 404(3).

Endres M., Fukuhara T., Pekker D., Cheneau M., Schau P., Gross C., Demler E., Kuhr S., and Bloch I. (2012). *The 'Higgs' amplitude mode at the two-dimensional superfluid/Mott insulator transition.* Nature, 487:454–458.

Feit M., Fleck J., and Steiger J. (1982). *Solution of the Schrödinger equation by a spectral method.* Journal of Computational Physics, 47(3).

Fertig C. D., O'Hara K. M., Huckans J. H., Rolston S. L., Phillips W. D., and Porto J. V. (2005). *Strongly inhibited transport of a degenerate 1D Bose gas in a lattice.* Phys. Rev. Lett., 94(120403).

Frisch O. R. (1933). *Experimenteller nachweis des Einsteinschen strahlungsruck-stosses.* Z. Phys., 86(42).

Gardiner C. and Zoller P. (2015). *The physics of quantum-optical devices*, volume 4. Imperial College Press.

Gati R. (2007). *A bosonic Josephson junction.* J. Phys. B, 40(10).

Geiger Z. A., Fujiwara K. M., Singh K., Senaratne R., Rajagopal S. V., Lipatov M., Shimasaki T., Driben R., Konotop V. V., Meier T., and Weld D. M. (2018). *Observation and uses of position-space Bloch oscillations in an ultracold gas.* Phys. Rev. Lett., 120(213201).

Giannakeas P., Melezhik V. S., and Schmelcher P. (2013). *Dipolar confinement-induced resonances of ultracold gases in waveguides.* Phys. Rev. Lett., 111(183201).

Goldman N., Juzeliūnas G., Öhberg P., and Spielman I. B. (2014). *Light-induced gauge fields for ultracold atoms.* IOP Science, 77(12).

Gould P. L., Lett P. D., and Phillips W. D. (1987). *New mea- surements with optical molasses,*. Springer-Verlag, Berlin, Laser Spectroscopy VIII(64).

Graham R., Schlautman M., and Zoller P. (1992). *Dynamical locaization of atomic-beam deflection by a modulated standing-wave*. Phys. Rev. A, 45(R19).

Grecchi V. and Sacchetti A. (1995). *Crossing and anticrossings of resonances: the Wannier- Stark ladder*. Annals of Physics, 241(258).

Greiner M., Bloch I., Mandel O., ansch T. W. H., and Esslinger T. (2001). *Exploring phase coherence in a 2D lattice of Bose-Einstein condensates*. Phys. Rev. Lett., 87(160405).

Greiner M., Mandel O., Esslinger T., HaEnsch T. W., and Bloch I. (2002a). *Collapse and revival of the matter wave field of a Bose-Einstein condensate*. Nature, 419(51).

Greiner M., Mandel O., Esslinger T., Hänsch T. W., and Bloch I. (2002b). *Quantum phase transition from a superfluid to a Mott Insulator in a gas of ultracold atoms*. Nature, 415(39).

Gross C. (2017). *Quantum simulations with ultracold atoms in optical lattices*. Science Journal, 357(6355):995–1001.

Habibian H., Winter A., Paganelli S., Rieger H., and Morigi G. (2013). *Bose-Glass phases of ultracold atoms due to cavity backaction*. Phys. Rev. Lett., 110(075304).

Hänsch T. W. (1975). *Cooling of gases by laser radiation*. Optics Communications, 13(1).

Hartmann T., Keck F., Korsch H. J., and Mossmann S. (2004). *Dynamics of Bloch oscillations*. New J. Phys., 6(2).

Heinze J., Krauser J. S., Fläschne N., Hundt B., Götze S., Itin A. P., Mathey L., Sengstock K., and Becker C. (2013). *Intrinsic photoconductivity of ultracold fermions in optical lattices*. Phys. Rev. Lett., 110(085302).

Holthaus M. (2000). *Bloch oscillations and Zener breakdown in an optical lattice*. J. Opt. B. Quantum Semiclass, 2(589).

Hooley C. and Quintanilla J. (2004). *Single-atom density of states of an optical lattice.* Phys. Rev. Lett., 93(080404).

Huckans J. H., Spielman I. B., Tolra B. L., Phillips W. D., and Porto J. V. (2009). *Quantum and classical dynamics of a Bose-Einstein condensate in a large-period optical lattice.* Phys. Rev. A, 80(043609).

Inouye S. M., Stenger A. J., Miesner H. J., Stamper-Kurn S., and Ketterle W. (1998). *Observation of Feshbach resonances in a BoseEinstein condensate.* Nature, 392(151).

Jaksch D. (2007). *Optical lattices, ultracold atoms and quantum information processing.* Contemporary Physics, 45(5):367–381.

Jaksch D. and Zoller P. (2004). *The cold atom Hubbard toolbox.* Annals of Physics, 315(1):52–79.

Jaynes E. T. and Cummings F. W. (1963). *Comparison of quantum and semiclassical radiation theories with application to the beam maser.* Proc. IEEE, 51(1):89–109.

Kapitza P. L. and Dirac P. A. M. (1933). *The reflection of electrons from standing light waves.* Proc. Cambridge Phil. Soc., 29(297).

Kolovsky A. R. and Korsch H. J. (2004). *Bloch osicillations of cold atoms In optical lattices.* Int. J. Modern Phys. B, 18(09).

Krieger J. B. and Iafrate. G. J. (1986). *Time evolution of Bloch electrons in a homogeneous electric field.* Phys. Rev. B, 33(5494).

Lebedev P. N. (1901). *Experimental examination of light pressure.* Ann. d. Phys. (Leipzig), 6(433).

Lebedev P. N. (1910). Ann. d. Phys. (Leipzig), 32(411).

Lee H. J., Adams C. S., Kasevich M., and Chu S. (1996). *Raman cooling of atoms in an optical dipole trap.* Phys. Rev. Lett., 76(2658).

Letokhov V. S. (1968). *Doppler line narrowing in a standing light wave.* JETP Lett., 7(272).

Letokhov V. S. and Minogin V. G. (1977). *Quantum motions of ultracooled atoms in resonant laser field*. Phys. Lett. A, 61(6).

Lewenstein M., Santos L., Baranov M. A., and Fehrmann H. (2004). *Atomic Bose-Fermi mixtures in an optical lattice*. Phys. Rev. Lett., 92(050401).

Longhi S. (2007). *Bloch dynamics of light waves in helical optical waveguide arrays*. Phys. Rev. B, 76(195119).

Louden R. (1983). *The quantum theory of light clerandon*. Oxford.

Mahmud K., Jiang L., Tiesinga E., and Johnson P. R. (2014). *Bloch oscillations and quench dynamics of interacting bosons in optical lattice*. Phys. Rev. A, 89(023606).

Marzari N., Mostofi A. A., Yates J. R., Souza I., and Vanderbilt D. (2012). *Maximally localized Wannier functions: Theory and applications*. Rev. Mod. Phys., 84(1419).

Mattis D. C. (1986). *The few-body problem on a lattice*. Rev. Mod. Phys., 58(361).

Medhat S., Yamakoshi T., Ayub M. A., Saif F., and Watanabe S. (2019). *Quantum suppresion of classical chaos in twinkling optical lattice*. (submitted).

Meixner J. and Schäfke F. W. (1954). *Mathieusche Funktionen und Sphroidfunktionen*. Springer-Verlag, Berlin.

Migdall A. L., Prodan J. V., Phillips W. D., Bergeman T. H., and Metcalf H. J. (1985). *First observation of magnetically trapped neutral atoms*. Phys. Rev. Lett., 54(2596).

Modugno G., de Mirandes E., Ferlaino F., Ott H., Roati G., and Inguscio M. (2004). *Atom interferometry in a vertical optical lattice*. Fortschr. Phys., 52(11-12):1173–1179.

Morsch O. and Oberthaler M. (2006). *Dynamics of Bose-Einstein condensates in optical lattices*. Rev. Mod. Phys., 78(179).

Nicholas E. F. and Hull G. F. (1903). *The pressure due to radiation*. Phys. Rev., 17(26).

Ott H., de Mirandes E., Ferlaino F., Roati G., Modugno G., and Inguscio M. (2004a). *Colli- Collisionally induced transport in periodic potentials.* Phys. Rev. Lett., 92(160601).

Ott H., de Mirandes E., Ferlaino F., Roati G., Türck V., Modugno G., and Inguscio M. (2004b). *Radio frequency selective addressing of localized atoms in a periodic potential.* Phys. Rev. Lett., 93(120407).

Palmer R. N., Klein A., and Jaksch D. (2008). *Optical lattice quantum Hall effect.* Phys. Rev. A, 78(013609).

Paredes B., Widera A., Murg V., Mandel O., Folling S., Cirac I., Shlyapnikov G. V., Hansch T. W., and Bloch I. (2004). *Tonks-Girardeau gas of ultracold atoms in an optical lattice.* Nature, 429(277).

Pedersen P. L., Gajdacz M., Winter N., Hilliard A. J., Sherson J. F., and Arlt J. (2013). *Production and manipulation of wave packets from ultracold atoms in an optical lattice.* Phys. Rev. A, 88(023620).

Pérez-Ríos J., Kim M. E., and Hung C.-L. (2017). *Ultracold molecule assembly with photonic crystals.* New J. Phys., 19(123035).

Pezzè L., Pitaevskii L., Smerzi A., Stringar S., Modugno G., de Mirandes E., Ferlaino F., Ott H., Roati G., and Inguscio M. (2004). *Insulating behavior of a trapped ideal Fermi gas.* Phys. Rev. Lett., 93(120401).

Polkovnikov A., Sachdev S., and Girvin S. M. (2002). *Nonequilibrium Gross-Pitaevskii dynamics of boson lattice models.* Phys. Rev. A, 66(053607).

Ponomarev A. V. and Kolovsky A. R. (2005). *Dipole and Bloch oscillations of cold atoms in a parabolic lattice.* Laser Physics, 16(2).

Raab E. L., Prentiss M., Cable A., Chu S., and Pritchard D. E. (1987). *Trapping of neutral sodium atoms with radiation pressure.* Phys. Rev. Lett., 59(2631).

Ramos A., Moore K., and Raithel G. (2017). *Measuring the Rydberg constant using circular Rydberg atoms in an intensity-modulated optical lattice.* Phys. Rev. A, 96(032513).

Rey A. M., Pupillo G., Clark C. W., and Williams C. J. (2005). *Ultracold atoms confined in an optical lattice plus parabolic potential: A closed-form approach*. Phys. Rev. A, 72(033616).

Roati G., D'Errico C., Fallani L., Fattori M., Fort C., Zaccanti M., Modugno G., Modugno M., and Inguscio M. (2008). *Anderson localization of a non-interacting Bose–Einstein condensate*. Nature, 453:895–898.

Ruuska V. and Törmä P. (2004). *Quantum transport of non-interacting Fermi gas in an optical lattice combined with harmonic trapping*. New J. Phys., 6(59).

Sacchetti A. (2017). *Bloch oscillations and accelerated Bose–Einstein condensates in an optical lattice*. Physics Letters A, 381(4).

Saif F. (2000). *Quantum recurrences: Probe to study quantum chaos*. Phys. Rev. E, 62(6308).

Saif F. (2005a). *Classical and quantum chaos in atom optics*. Physics Reports, 425(5-6).

Saif F. (2005b). *Nature of quantum recurrences in coupled higher dimensional systems*. Eur. Phys. J. D, 39(87-91).

Saif F. and Watanabe S. (2019). *Optical forces on atoms*. IOP Publishing.

Schneider P. I. (2012). *Quantum computation with ultracold atoms in a driven optical lattice*. Phys. Rev. A, 85(050304).

Sherson J. F., Park S. J., Pedersen P. L., Winter N., Gajdacz M., Mai S., and Arlt J. (2012). *The pump–probe coupling of matter wave packets to remote lattice states*. New J. Phys., 14(083013).

Tayebirad G., Zenesini A., Ciampini D., Mannella R., Morsch O., Arimondo E., Lörch N., and Wimberger S. (2010). *Time-resolved measurement of Landau-Zener tunneling in different bases*. Phys. Rev. A, 82(013633).

Theis M., Thalhammer G., Winkler K., Hellwig M., amd R. Grimm G. R., and Denschlag J. H. (2004). *Tuning the scattering length with an optically induced Feshbach resonance*. Phys. Rev. Lett., 93(123001).

Viverit L., Menotti C., Calarco T., and Smerzi A. (2004). *Efficient and Robust Initialization of a Qubit Register with Fermionic Atoms.* Phys. Rev. Lett., 93(110401).

Wannier G. (1960). *Wave functions and effective hamiltonian for bloch electrons in an electric field.* Phys. Rev., 117(432).

Wannier G. H. (1937). *The Structure of Electronic Excitation Levels in Insulating Crystals.* Phys. Rev., 52(191).

Westbrook C. I., Watts R. N., Tanner C. E., Rolston S. L., Phillips W. D., Lett P. D., and Gould P. L. (1990). *Localization of atoms in a three-dimensional standing wave of light.* Phys. Rev. Lett., 65(33).

Wineland D. J. (1975). *Principles of the stored ion calorimeter.* Journal of Applied Physics, 46(919).

Yamakoshi T., Saif F., and Watanabe S. (2018). *Significantly stable mode of the ultracold atomic wave packet in amplitude-modulated parabolic optical lattices.* Phys. Rev. A, 97(023620).

Yamakoshi T. and Watanabe S. (2015). *Single-particle analysis of non-interacting ultracold bosons in amplitude modulated parabolic optical lattice.*

Yamakoshi T., Watanabe S., Ohgoda S., and Itin A. P. (2016). *Dynamics of fermions in an amplitude modulated lattice.*

Zener C. (1932). *Non-adiabatic crossing of energy levels.* Proc. R. Soc. A, 137(696).

Zener C. (1934). *A theory of the electrical breakdown of solid dielectrics.* The Royal Society, 145(855).

Zohar E., Cirac J. I., and Reznik B. (2015). *Quantum simulations of lattice gauge theories using ultracold atoms in optical lattices.* IOP Science Journal, 79(1).